Distribution Agreement

In presenting this thesis or dissertation as a partial fulfillment of the requirements for an advanced degree from Emory University, I hereby grant to Emory University and its agents the non-exclusive license to archive, make accessible, and display my thesis or dissertation in whole or in part in all forms of media, now or hereafter known, including display on the world wide web. I understand that I may select some access restrictions as part of the online submission of this thesis or dissertation. I retain all ownership rights to the copyright of the thesis or dissertation. I also retain the right to use in future works (such as articles or books) all or part of this thesis or dissertation.

Signature:

_____ _____

Elizabeth A. Baker Date

Physical Aging of Confined Polymer Films by Use of a New Streamlined Ellipsometry Procedure

By

Elizabeth A. Baker

Master of Science, Physics

(Connie B. Roth)

Advisor

(Justin Gallivan)

Committee Member

(Kurt Warncke)

Committee Member

(Eric Weeks)

Committee Member

Accepted:

(Lisa A. Tedesco, Ph.D.)

Dean of the Graduate School

(Date)

Physical Aging of Confined Polymer Films by Use of a New Streamlined Ellipsometry Procedure

By

Elizabeth A. Baker

B.S., Bucknell University, 2006

Advisor: Connie B. Roth, Ph.D.

An abstract of a thesis

submitted to the Faculty of the

Graduate School of Emory University

in partial fulfillment of the requirements for the degree of

Master of Science in Physics

2009

Abstract

Physical Aging of Confined Polymer Films by Use of a New Streamlined Ellipsometry Procedure

By

Elizabeth A. Baker

A new streamlined ellipsometry procedure for measuring the physical aging of confined polymer films is discussed. Supported polystyrene films both bulk (2.5 μm) and thin (down to 30 nm) on native silicon were used to test this ellipsometry procedure. Four different methods to calculate the physical aging rate, β, of these confined polymer films are compared: one method involving Struik's original definition of physical aging rate, one method involving the height of the polymer film normalized at 10 minutes into the run h_0, one method involving the Lorentz-Lorenz equation, and a final method which uses the thermal expansion coefficient of a glassy polymer film and the change in the index of refraction over time. Using these four methods on the supported polystyrene films, the calculated physical aging rate produces curves of physical aging rate against aging temperature characteristic of those in the literature. The second method out of four is chosen, $\beta = -(1/h_0)(\partial h/\partial \log t)$, as the best way to measure the physical aging rates of confined polymer films. Furthermore, the experimental time is optimized to 360 minutes of physical aging. The dependence of physical aging rate on film thickness is also tested. Below 100 nm in film thickness, a decrease in physical aging rate with decreasing film thickness is observed. This behavior may be explained by a gradient in the physical aging rate as a function of depth, as has been previously reported in the research literature. Now that it is known that the new ellipsometry procedure correctly characterizes the physical aging of supported polystyrene films, the physical aging behavior of different polymers in a supported state can be tested, as well as the physical aging of polystyrene in a free-standing state.

Physical Aging of Confined Polymer Films by Use of a New Streamlined Ellipsometry Procedure

By

Elizabeth A. Baker

B.S., Bucknell University, 2006

Advisor: Connie B. Roth, Ph.D.

A thesis submitted to the Faculty of the

Graduate School of Emory University

in partial fulfillment of the requirements for the degree of

Master of Science in Physics

2009

Contents

List of Figures

List of Tables

Chapter 1

Introduction

Polymers are macromolecules with diverse applications in biological, medical, and commercial fields. They are composed of chains of single units called monomers. Their versatility means that they are found in almost every part of nature. However, over time the polymer will age, become brittle, and less able to complete its assigned tasks.

The physical aging (stability) of polymers in the glassy state in confined systems is very important. Polymers increasingly are located in confined states, especially for applications in nanotechnology, nanocomposites, and ultrathin gas separation membranes [1]. However, the physical properties of a polymer in its confined state are different from those in its bulk state. In this thesis, a new method to measure the physical aging rate of thin polymer films using ellipsometry is described, similar to methods used by Huang and Paul [2] and Richardson et al. [3].

1.1 Glass Transition in Polymers

Because it is difficult to induce a polymer into a crystalline state, almost all polymers enter a glassy state upon cooling [4]. Figure 1.1 shows a schematic of how the volume of a polymer varies with temperature upon cooling. If the polymer begins

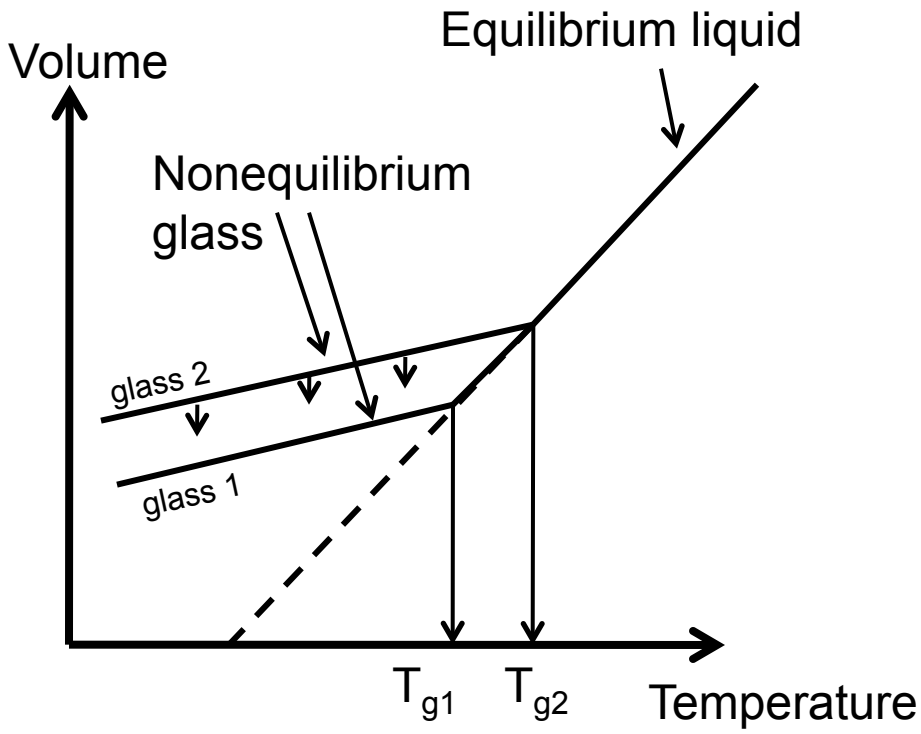

Figure 1.1: This schematic depicts the change in volume with temperature for a polymer [4]. Beginning in an equilibrium liquid state, if the polymer is cooled slowly, it will undergo a transformation at T_{g1}, its glass transition temperature, and enter a nonequilibrium glassy state (glass 1). If the polymer is instead cooled quickly (quenched), it will become glassy at a higher glass transition temperature T_{g2}, and form a glassy state with a higher volume (glass 2). Since glass 2 has a higher volume than glass 1, it will attempt to achieve a lower volume by tiny volume relaxations below the glass transition temperature, represented by the tiny downwards arrows descending from glass 2. This process is referred to as structural relaxation or physical aging [5–9].

in an equilibrium liquid state and is cooled slowly, it will transform into a glass at a given temperature, glass 1. The temperature at which this transformation occurs is called the glass transition temperature T_{g1}. However, if the glass is cooled rapidly (quenched) it will form a glass with a higher volume (glass 2) at a higher glass transition temperature T_{g2}. Glass 2 occupies a higher volume than glass 1, so it will attempt to reach the state of glass 1 through tiny volume relaxations, visually represented by the tiny downwards arrows from glass 2 in Figure 1.1. These tiny volume relaxations

depend in part on the mobility of segments of polymer chains collapsing into pockets of available free volume [10]. This process is referred to as structural relaxation or physical aging [5–9].

The change in glass transition temperatures with polymer film thickness has received great attention in the literature [11–16]. For polystyrene (PS) in particular, it is known that the glass transition temperature decreases with decreasing film thickness for films less than approximately 100 nm thick [11, 14–17]. It is also known that the decrease in glass transition temperature occurs more rapidly for free-standing PS films compared to supported PS films [13]. Furthermore, Ellison and Torkelson found for supported PS films not a single glass transition temperature but a gradient of different glass transition temperatures as a function of depth from the free surface [16]. This indicated regions of different mobility for segments of polymer chains [16]. A gradient in physical aging rate with depth has been observed in poly(methyl methacrylate) (PMMA) films through the experiments of Torkelson and coworkers [17].

1.2 Physical Aging in Bulk Polymers

Physical aging is the process of tiny volume relaxations in the polymer over time at a temperature below T_g [5–9]. The process is inherently reversible: if the glassy polymer is heated above T_g and allowed to thermally equilibrate all previous thermal history will vanish [5–9]. The problem with physical aging is that it causes material to become brittle and wear out.

Tiny volume changes from physical aging result in huge changes in the properties of the polymer [8]. Observe Figure 1.2, which shows the change in specific volume (1/density) plotted against temperature for a 400 nm polysulfone (PSF) film [18]. The solid lines and dotted line seen in the figure are identical to those in Figure 1.1. A single point on the graph indicates the occupied volume of the polymer film V_0.

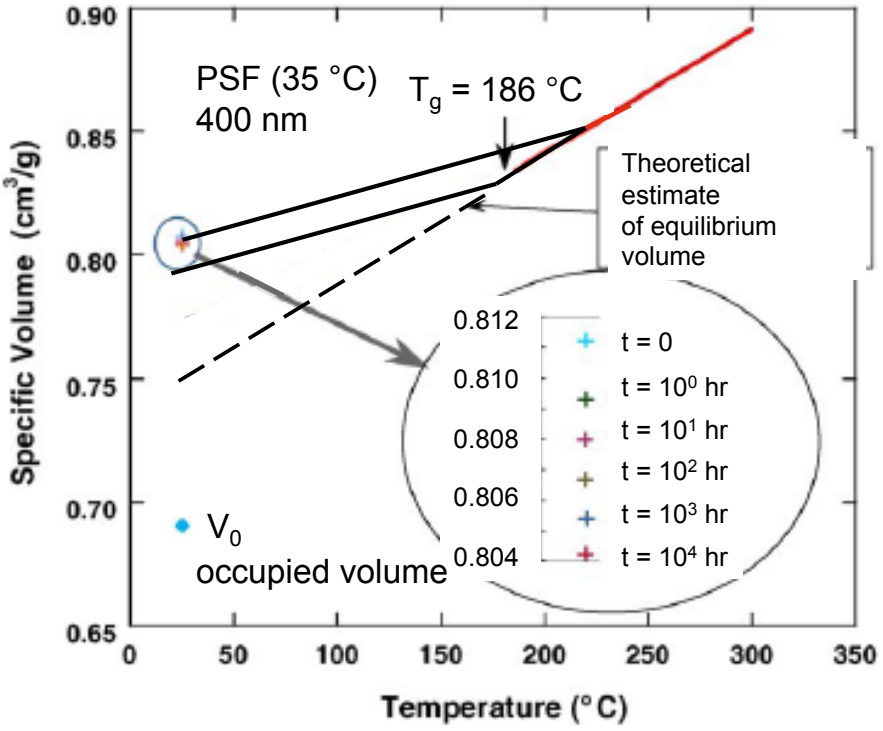

Figure 1.2: This figure shows the changes in specific volume over temperature of a 400 nm polysulfone film aged at 35 °C for 10,000 hours, or ∼1 year [18]. The resulting changes in specific volume over this aging time are displayed in the circled inset. V_0 is the occupied volume of the molecules composing the polymer chains. The three solid lines and dotted line are the same as seen in Figure 1.1. (Figure modified from ref. [18].)

The inset of the graph depicts the changes in the specific volume over an aging time of 10,000 hours, (∼1 year), when aged at 35 °C. Even over a year of physical aging time, the polymer has not reached the theoretical equilibrium glassy volume, much less the occupied volume of the polymer. Physical aging this far below the glass transition temperature of PSF (T_g = 186 °C) means these volume changes are so tiny as to be barely detectable (inset of Figure 1.2). However, it has been reported that PSF films lose 75% of their permeability to CH_4 in the space of one year [19]. These changes in volume are extremely tiny, but still strongly affect the permeability, brittleness, modulus, and stiffness of the polymer [8].

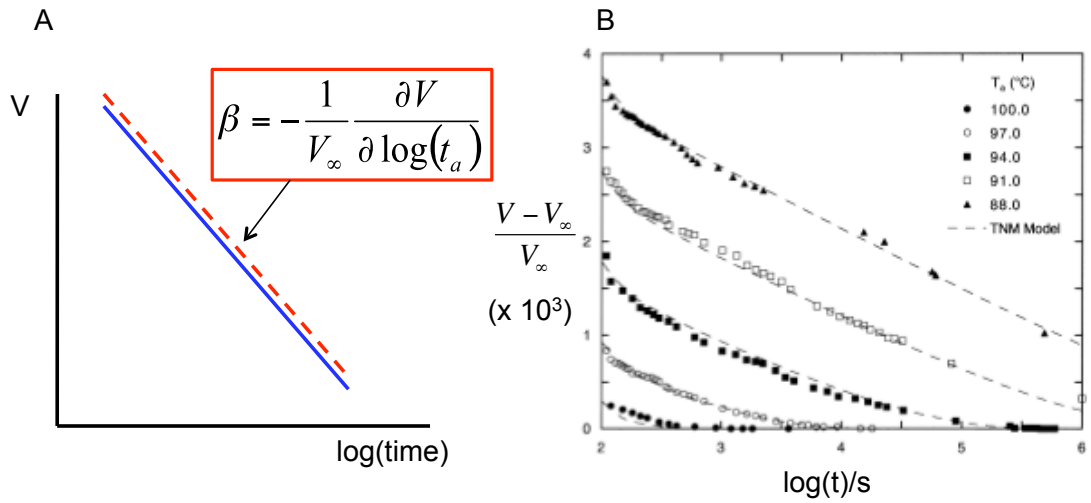

Figure 1.3: (A) This schematic depicts the changes of volume normalized by the theoretical equilibrium volume V_∞ over the logarithmic time of a polymer. A slope fit to the data (dotted line) gives the physical aging rate β [6]. (B) This figure shows how volume normalized by V_∞ of polystyrene changes over logarithmic time when quenched to different aging temperatures [20]. At each temperature, the data can be fit to a linear model as in (A), except when nearing equilibrium [1,20]. (Figure shown with permission from ref. [20]).

Physical aging rates can be measured by fitting a slope to a graph of volume, normalized by the theoretical equilibrium volume V_∞, versus time [20]. Observe Figure 1.3 (A), which depicts a schematic of volume plotted against the logarithmic time of a polymer undergoing physical aging. The slope fit to the data gives the physical aging rate, β. This physical aging rate is defined by Struik as,

$$\beta = -\frac{1}{V_\infty}\frac{\partial V}{\partial \log t}, \tag{1.1}$$

where V_∞ is the theoretical equilibrium volume of the polymer if it could be cooled infinitely slowly [6]. Compare the sketch with Figure 1.3 (B), a graph of the change of normalized volume of polystyrene over time when quenched to various aging temperatures [20]. A fit to the linear portions of the data will give the physical aging rate at a given aging temperature [20]. The volume measurements in Figure 1.3 (B)

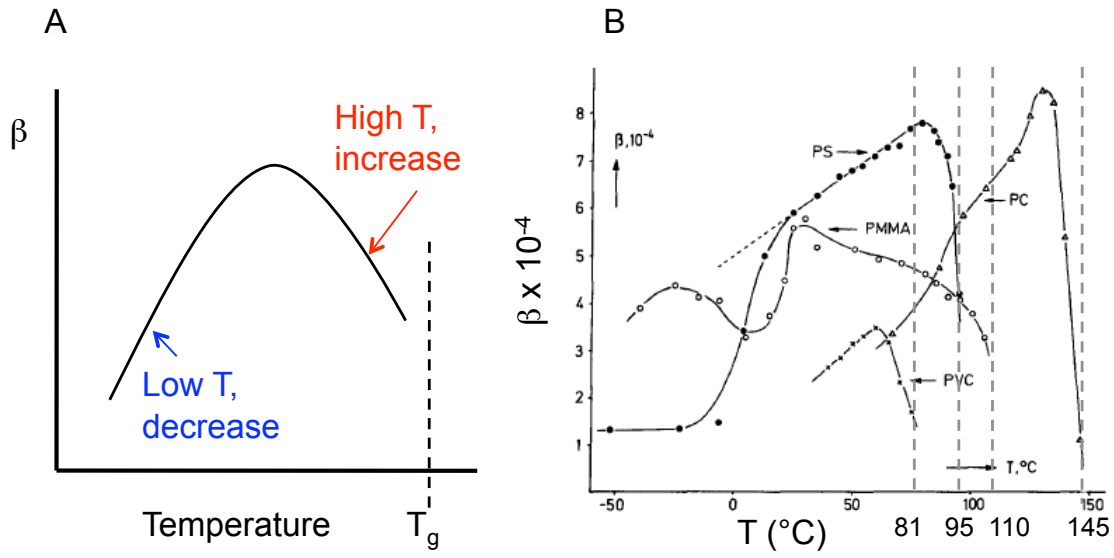

Figure 1.4: (A) This schematic depicts the changes in the physical aging rate β over temperature for a polymer. At aging temperatures just below the glass transition temperature, as the aging temperature decreases, the polymer chains are driven to contract together, so β increases with decreasing aging temperature. At low aging temperatures, as the aging temperature decreases, there is less thermal energy available for the segments of the polymer to contract, so the physical aging rate decreases with decreasing temperature. The combination of these two effects gives the curve. (B) This graph shows the measured change in physical aging rate with temperature for four different polymers: PS, PMMA, poly(vinyl chloride) (PVC), and polycarbonate [21]. Each curve has the characteristic shape of the schematic except for PMMA, which has an unusual secondary transition at low aging temperatures (Figure used with permission from ref. [21]).

were taken using dilatometry measurements, which directly measures the changes in volume of a bulk polymer sample [4].

The physical aging rate also changes depending on the aging temperature [5–9]. Figure 1.4 (A) is a schematic depicting the change in physical aging rate β with aging temperature. At high aging temperatures, as the temperature decreases, the difference in between the measured volume V and the theoretical equilibrium volume V_∞ increases, increasing the driving force towards densification. Thus, as the temperature decreases, the physical aging rate increases. At low aging temperatures, as the temperature decreases, less thermal energy is available to allow the segments

of the polymer chains to move, so the physical aging rate decreases with decreasing aging temperature. The combination of these two effects produces the physical aging curve shown in the schematic. Physical aging can only occur beneath the glass transition temperature of a polymer. In Figure 1.4 (B) curves of physical aging rate vs. time are shown for several different polymers: PS, PMMA, poly(vinyl chloride) (PVC), and polycarbonate (PC) [21]. All four curves follow the same shape as the schematic, except PMMA, which has an unusual secondary transition at very low aging temperatures [21].

1.3 Physical Aging in Thin Polymer Films

When polymer films are made thin (confined state), there are two different observed changes in the physical aging rate. One group of observations reveals accelerated physical aging with decreasing film thickness [2, 18, 19, 22–28]. The other group of observations reveals either no change or even suppressed physical aging with decreasing film thickness [17, 29–31]. Polymers can be classified into two different groups to attempt to make sense of these different observations. As seen in Figure 1.5, one group has flexible C-C backbones, which can bend easily and pack together fairly well. The other group has monomers with large aromatic rings along the backbone, making them stiff. This group is known as "high free volume" or stiff-backbone polymers. Figure 1.5 is not an official classification of polymers, but a grouping based on different physical backbone structures as a means of interpreting the two different observations.

1.3.1 Physical Aging in Thin Polymer Films, Stiff-Backbone

Gas permeation experiments on stiff-backbone polymer films of varying film thickness produced some of the earliest observations of accelerated physical aging [26–28]. The

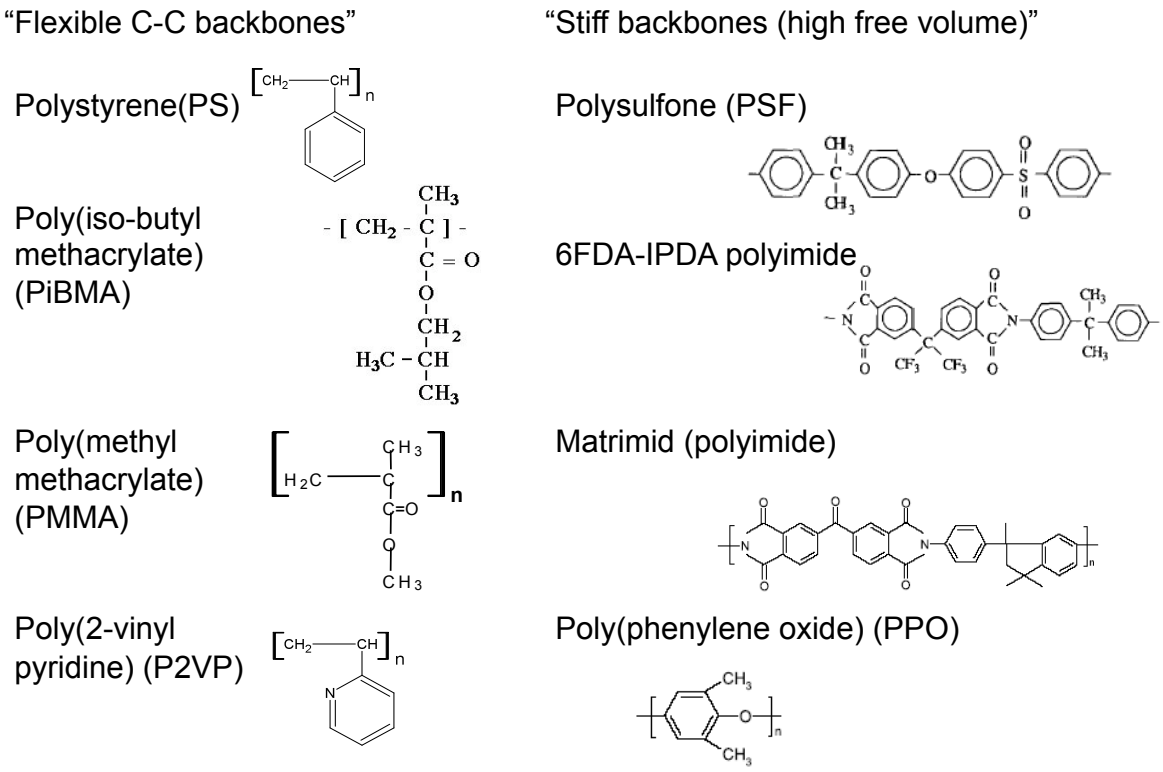

Figure 1.5: This figure shows the way in which polymers are classified in this thesis in order to try and understand the different observed changes in the physical aging rate with decreasing film thickness. Flexible backbone polymers have only carbons along their backbones and are able to pack together fairly well. Stiff backbone polymers have bulky rings in their backbones, and do not pack together well. They are known as "high free volume" polymers by the gas permeation community.

permeability P of the material is determined by the ability of a gas to adsorb to the surface of the material (controlled by sorption S) and then diffuse through the material (controlled by diffusion D) following the form $P = DS$ [32]. The units of permeability are listed in Barrers (1 Barrer = 10^{-10}cm^3(STP)cm/cm^2) [26]. Since diffusion relies on the free volume between the polymer chains, and that volume decreases over time during physical aging, gas permeation measurements are a sensitive way to measure physical aging of a polymer. The earliest gas permeation physical aging measurements were performed by Pfromm and Koros on polyimide and PSF using a porous ceramic support disc [26]. Using a ceramic disc support meant that the observed accelerated physical aging at decreasing film thicknesses was not due to collapse of the underlying support, but rather entirely due to the physical aging of the polymer film [26]. This confirmed the first observation of accelerated physical aging with decreasing film thickness in polymer films [26].

Huang and Paul investigated the physical aging of "high free volume" polymers of varying film thickness using both gas permeation and ellipsometry measurements [2, 18, 19, 22–24]. Observe Figure 1.6 (A), which depicts the change in oxygen gas permeability of PSF films aged at 35 °C for 10,000 hours (∼1 year) [24]. For the very thickest films (∼60 μm), the decrease in the permeability of the polymer over the aging time is about 10% [24]. However, for the thinnest films (∼1000 nm or less), this decrease in the permeability over the aging time is closer to 50% [24]. This provides evidence of accelerated physical aging for thin polymer films. Figure 1.6 (B) depicts the same polymer aged over the same aging time at the same aging temperature, only monitoring the change in the index of refraction over logarithmic time [23]. Again, as the film thickness decreases the change between the initial and final values of the measured parameter increases [23].

The ellipsometry procedure used by Huang and Paul [2] to measure the physical aging of polymer films begins by spincoating polymer in solution onto silicon wafers,

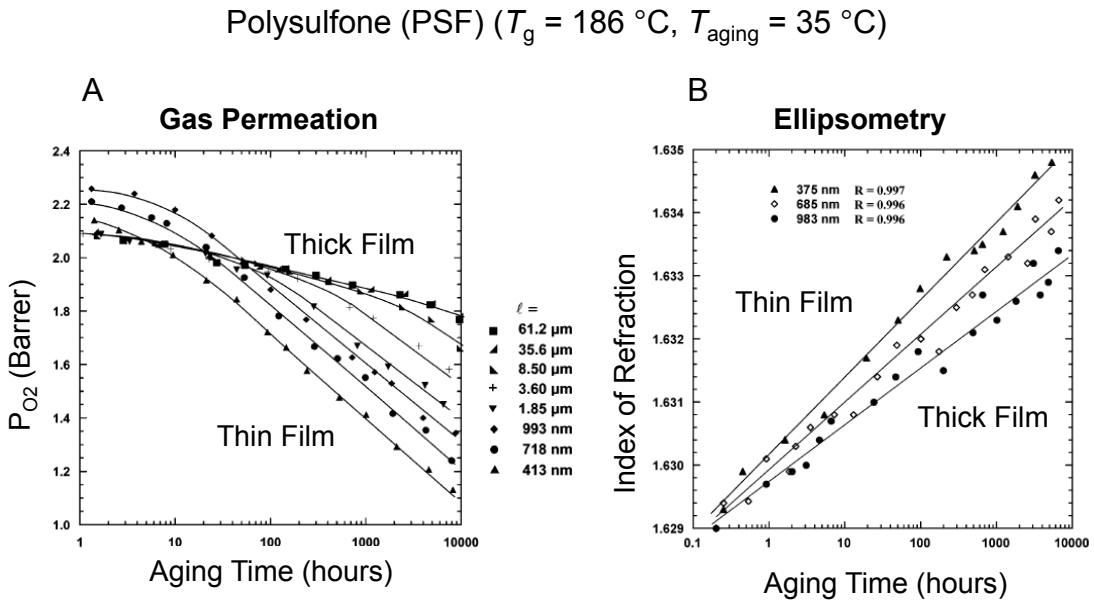

Figure 1.6: Both of these figures measure changes in properties of PSF films aged at 35 °C for 10,000 hours. (A) This figure depicts the changes in oxygen permeability over the aging time for PSF films of various thicknesses [24]. For the very thickest films ($\sim$60 μm), the change in the permeability over the whole aging time decreases by 10%. However, for the thinnest films ($<\sim$1000 nm), that decrease in the permeability is closer to 50%. (Figure used with permission from ref. [24]). (B) This figure depicts the change in the index of refraction over logarithmic aging time for PSF films of various film thicknesses [23]. Again, as the film thickness decreases, the change in between the initial and final values of the measured parameter increases over the aging time. (Figure used with permission from ref. [23]).

then transferring the polymer films onto rectangular wire frames. The films are placed in such a way as to be supported only on two sides. A film is then heated above T_g, allowed to thermally equilibrate, and quenched in a free-standing state. The film is gently rolled onto a silicon wafer, taken to the ellipsometer, and its index of refraction measured. The film is then placed in an oven at the aging temperature, under a nitrogen gas atmosphere, until the next measurement. These measurements were repeated every few days or so over the whole aging time. Through this method, optically-based measurements (ellipsometry) were able to confirm the observations of gas permeation-based measurements: accelerated physical aging in polymer films with decreasing thickness.

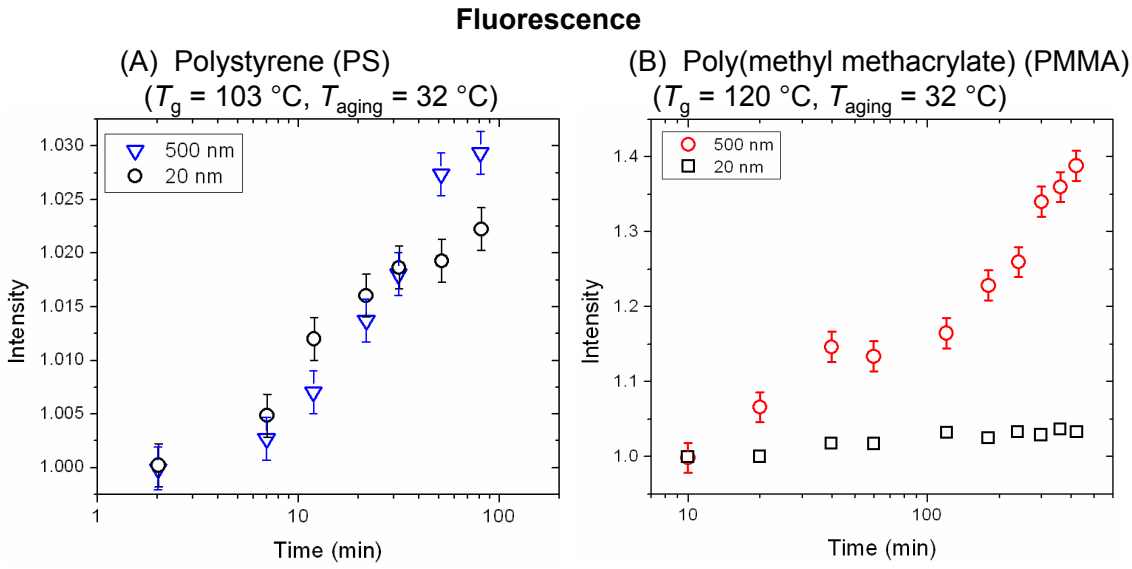

Figure 1.7: (A) This figure shows the change in intensity over time of supported PS films aged at 32 °C for two different film thicknesses: 500 nm thick (triangles) and 20 nm thick (circles) [30]. There is no significant difference in the change in intensity for the 20 nm thick film compared to the 500 nm thick film. (B) This figure shows the change in intensity over time of PMMA films aged at 32 °C measured at two different film thicknesses: 500 nm (circles) and 20 nm (squares) [30]. The film at 20 nm shows suppressed physical aging compared to that at 500 nm. (Data replotted from ref. [30]).

1.3.2 Physical Aging in Thin Polymer Films, Flexible C-C Backbone

No change or suppressed physical aging rates with decreasing film thickness were observed from work by Torkelson and coworkers [17, 29, 30, 33]. They measured the physical aging of polymer films using fluorescence [17, 29, 30, 33, 34]. The fluorescent probes, Julolidene malononitrile (JMN) or 4-tricyanovinyl-[N-(2-hydroxyethyl)-N-ethyl]aniline (TC1) for example, are designed to detect the changes in the local volume surrounding the probe [17, 29, 30, 34]. As physical aging proceeds, the ability of these so-called 'rotor' probes to rotate becomes hindered as the free volume decreases, causing their fluorescence intensity to increase over aging time [17, 30, 34].

Fluorescence experiments have revealed either no change [29,30] in physical aging

or suppressed [17, 33] physical aging with decreasing film thickness. Figure 1.7 (A) depicts changes in intensity received from fluorescent probes in 500 nm and 20 nm thick PS films plotted against logarithmic aging time [30]. Over the aging time there is little significant difference in the change in intensity over time of the 20 nm thick PS film compared with the 500 nm thick PS film. Poly(methyl methacrylate) films show a different behavior when the changes in intensity over logarithmic time is measured for films 500 nm thick and 20 nm thick. Figure 1.7 (B) shows the change in intensity over logarithmic time for 500 nm thick and 20 nm thick PMMA films. The 20 nm thick film shows a distinct suppression in physical aging compared to the 500 nm thick film. This effect is suspected to be caused by the attraction between the hydroxyl groups on the native oxide surface of the silica substrate and the ester groups of the PMMA [17, 31]. Thus, suppressed physical aging can be observed with decreasing film thickness using fluorescence measurements.

1.3.3 Possible Source of the Differences in Physical Aging in Thin Polymer Films

Are these differences in the physical aging rates with confinement caused by the structure of the polymer itself? Based on the chemical structure of the polymer alone, accelerated physical aging in confinement has been observed in stiff-backbone polymer films, while no change or suppressed physical aging in confinement has been observed in flexible C-C backbone polymer films. Experimentally, gas permeation and ellipsometry experiments detected accelerated physical aging, while fluorescence measurements detected either no change or suppressed physical aging. In addition, experiments which indicate accelerated physical aging use films which are measured (or at least quenched) in a free-standing state. No change or even suppressed physical aging is seen for films measured and quenched in a supported state. There are no attractive interactions present for a polymer which undergoes accelerated physical

aging, while attractive interactions of the polymer with the substrate are present when suppressed physical aging is observed.

Another difference between these studies is the length scale at which the physical aging rate is observed to change. Physical aging rate changes in free-standing polymer films were observed to occur well above 10 μm in film thickness [24]. In supported polymer films, these changes occur at film thicknesses of 250 nm or less [17]. The length scale of both of these changes, however, is different from the length scale at which changes in the glass transition temperature take place, typically $< \sim$100 nm [14, 17]. Use of a single experimental technique will remove the experimental differences associated with all the different techniques and allow the ability to focus on the changes of the physical aging rate based on the structure of the polymer. The long term goal is to determine if the physical aging rates of confined films is dependent on polymer structure alone. This will reside with future work. For this thesis, the first step was to decide on an experimental technique.

Two previous attempts to measure the physical aging rate of polymer films with both types of backbones have been previously attempted by Connie Roth and Perla Rittigstein. First, an attempt was made with fluorescence measurements to detect the physical aging of PSF films. During the heating phase of the experiment, however, the dye sublimated out of the film and no measurements were able to be recorded [10]. Second, gas permeation measurements were performed on PMMA films. Unfortunately, no change in the permeability was observed with film thickness (800 μm to 190 nm) or length of aging time (up to 65 days) [10]. Thus, ellipsometry was selected as the most promising experimental technique to be able to measure both flexible C-C backbone and stiff-backbone polymers.

1.4 Scope of Thesis

This thesis demonstrates the results of physical aging experiments performed on supported polystyrene films using a new streamlined ellipsometry procedure. Beginning with bulk PS films ∼2500 nm thick supported on silicon with the native oxide intact, ellipsometry is shown to be capable of characterizing the physical aging rate of PS with temperature. Four different ways to calculate the physical aging rate are tested and a single one, $\beta = -(1/h_0)(\partial h/\partial \log(t))$, is chosen as the best one out of the four for the purposes of the experiments. The time over which aging occurred was also optimized to 360 minutes from an original time of 24 hours. Physical aging measurements of PS films with decreasing film thickness were also performed. A decrease is seen in the physical aging rate with a decrease in film thickness for PS film thicknesses below 100 nm. It was found that this does not correspond to a simple decrease in glass transition temperature [10]. However, this decrease in physical aging rate with film thickness could be modeled using a bilayer film with a thin liquidlike surface layer [10]. Future work will consist of applying the new ellipsometry procedure to detect physical aging rates of different polymers and testing the physical aging rate of PS in a free-standing state.

Chapter 2

Experimental Techniques

2.1 Sample Preparation

Polystyrene films were produced by spincoating polymer solution onto silicon wafers. The polymer solution was prepared by mixing polystyrene (Sigma-Aldrich, Mw = 280,000, secondary standard) with toluene. Solutions ranged from concentrations of 1 wt% to 15 wt%.

Each polymer solution was spin-coated onto 2 cm x 2 cm native silicon wafers with the natural silicon oxide layer (2 nm thick) intact. Spin speeds ranging from 500 rpm to 3000 rpm were used to achieve film thicknesses from as thick as 2700 nm to as thin as 30 nm. After spincoating, these films were placed into a vacuum oven at (120 ± 3) °C, above their measured T_g of (97 ± 2) °C. The films were annealed under vacuum above T_g for at least 12 hours before being used for aging experiments.

2.2 Rotating Compensator Ellipsometer

A rotating compensator ellipsometer (J. A. Woollam M2000D) was used to measure the changes in film thickness and index of refraction of the polymer films over time. The ellipsometer obtains measurements of film thickness and index of refraction by

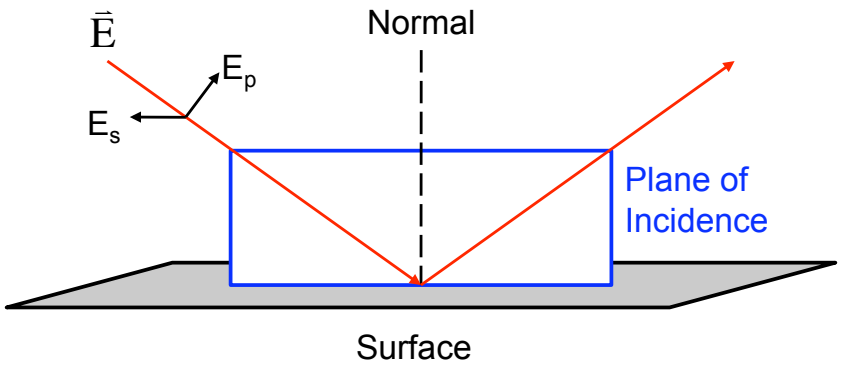

Figure 2.1: This picture shows the path of a beam of light with electric field $\vec{E}$ as it reflects from a surface [35]. The plane of incidence is defined as the plane which contains the path of the light approaching towards the surface, reflecting from that surface, and the normal to that surface. This electric field has two components. One component is polarized parallel to the plane of incidence E_p, and the other component is polarized perpendicular to the plane of incidence E_s [35].

measuring the change in the state of the polarization of light upon reflection from the sample [36]. A schematic of a beam of light interacting with the surface is given in Figure 2.1. The electric field of the incident beam of light $\vec{E}$ can be split into two parts, E_p, parallel to the plane of incidence, and E_s, perpendicular to the plane of incidence [35–37],

$$\vec{E} = E_s\hat{x} + E_p\hat{y}, \tag{2.1}$$

$$|E_{total}| = \sqrt{|E_p|^2 + |E_s|^2}. \tag{2.2}$$

The important part of Figure 2.1 is the visual representation of the plane of incidence, defined by the incoming beam of light, the reflected beam of light, and the normal to the surface. The fundamental formula of ellipsometry governing the change in polarization is

$$\frac{r^p_{tot}}{r^s_{tot}} = \rho = \tan\psi e^{i\Delta}, \tag{2.3}$$

where r^p_{tot} is the total Fresnel reflection coefficient polarized in the direction parallel to the plane of incidence p, r^s_{tot} is the total Fresnel reflection coefficient polarized in

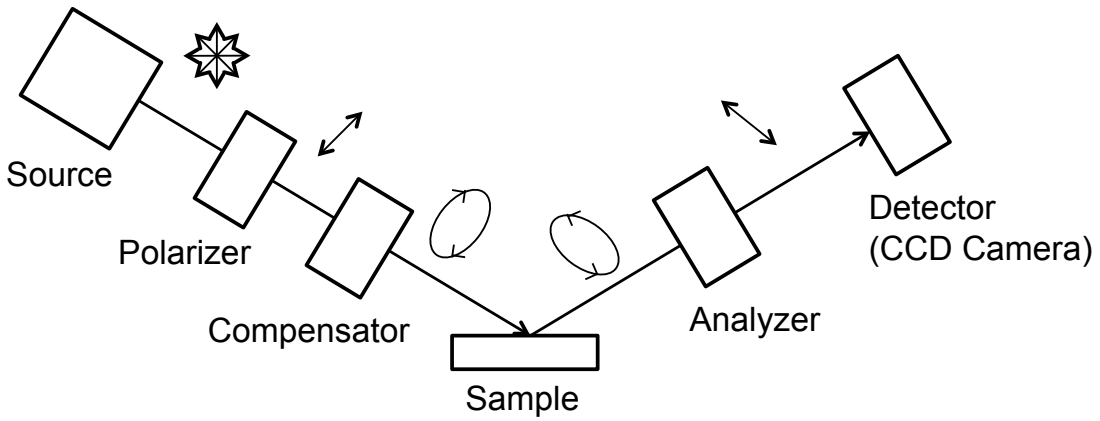

Figure 2.2: This picture shows a schematic of the components for the rotating compensator ellipsometer [36]. Light travels from left to right in the figure, originating in the source lamps and ending at the CCD camera. The polarization state of the light is represented by the small figures above the path of light between each optical component. The light exits the source (D2 and QTH lamps) as unpolarized light. The polarizer and analyzer both translate incoming beams of light into linearly polarized light. The compensator translates this light into elliptically polarized light. The intensity of the resultant light is analyzed by a CCD camera, capable of detecting multiple wavelengths of light at once. The resulting information is relayed to the computer, where it can be analyzed.

the direction perpendicular to the plane of incidence s, ψ is an amplitude and Δ a phase [36,37]. The origin of Equation (2.3) and knowledge of the optical components of the ellipsometer are necessary in order to understand how the ellipsometer is able to measure ψ and Δ and relate these values to the desired quantities of film thickness h and index of refraction n of the film.

2.2.1 Components of Ellipsometer

There are five different optical components of the ellipsometer, depicted in a schematic in Figure 2.2 [36,37]. For the M2000D ellipsometer, the light originates from two different bulbs: a D2 deuterium lamp and a quartz-tungsten-halogen (QTH) lamp, which collectively produce unpolarized light from 193 nm to 1000 nm in wavelength [38]. This unpolarized light travels to the polarizer, an optical element which makes the

incoming light linearly polarized [36]. This linearly polarized light interacts with the rotating compensator, which transforms the linearly polarized light into elliptically polarized light by slowing down one of its components (E_p or E_s) with respect to the other [35–37]. This elliptically polarized light then interacts with the sample and reflects from it as a different beam of elliptically polarized light. The resulting light passes through a second polarizer (called the analyzer), which returns the state of the light to linearly polarized [36, 37]. Finally the light is detected by a CCD camera, which has the capability of analyzing multiple wavelengths of light simultaneously [36]. The information from this detector is relayed to the computer, where it can be analyzed.

2.2.2 Relevant Equations of Ellipsometry

The complex index of refraction $\widetilde{n}$ is composed of the real part of the index of refraction n and the absorption coefficient k [37, 39],

$$\widetilde{n} = n + ik. \tag{2.4}$$

Besides the silicon substrate, none of the other components of a supported polymer film from the experiments presented in this thesis contain an imaginary part of the index of refraction k. The index of refraction of polystyrene, for example, varies from 1.55-1.59 [40]. It should also be noted that the index of refraction n and absorption coefficient k vary with wavelength λ. The change in index of refraction and absorption coefficient for the silicon substrate and native silicon oxide layer is depicted in Figure 2.3 [41]. For a nonzero n or k, the dependence of index of refraction and absorption coefficient have the form of a $1/\lambda^d$ polynomial function, where d is a positive integer greater than one [41]. For the purposes of the derivation, the existence of the native oxide layer will be temporarily ignored.

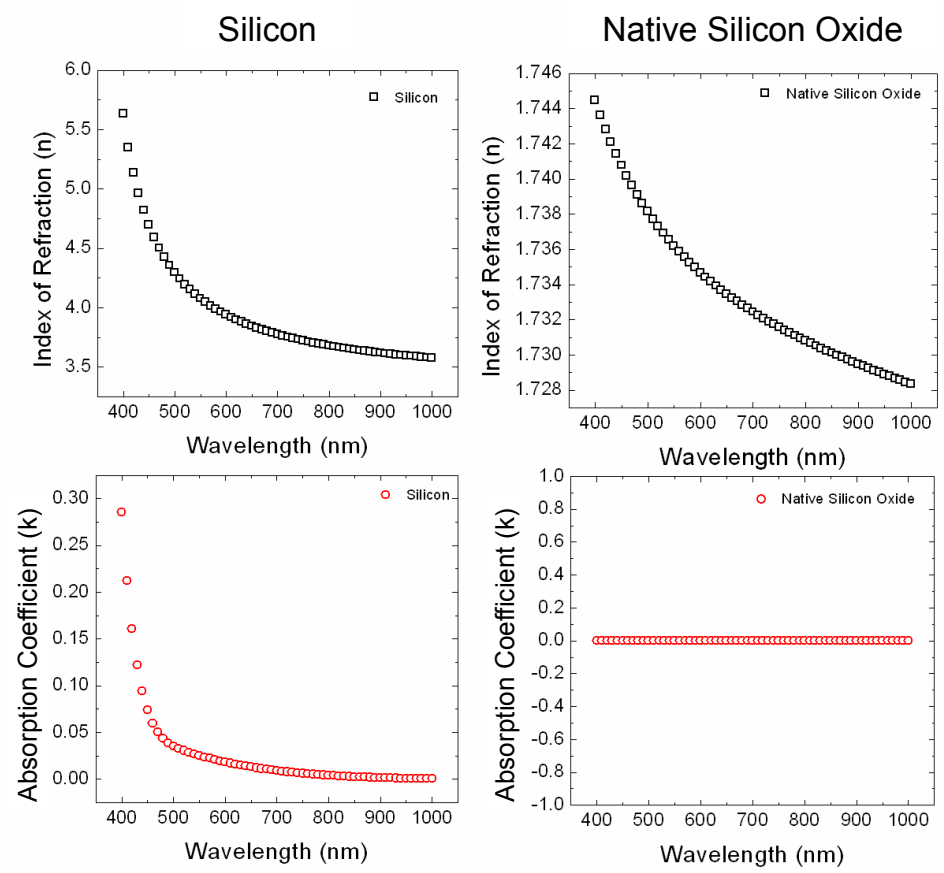

Figure 2.3: These graphs depict how the real (n) (squares) and imaginary (k) (circles) parts of the complex index of refraction $\widetilde{n}$ for silicon (left) and native silicon oxide layers (right) vary over the wavelength λ [41]. Only the silicon substrate contains a nonzero absorption coefficient k in the supported film experiments of this thesis.

The film thickness h and index of refraction n of a thin film can be related to the two measured values from the ellipsometer, ψ and Δ. To accomplish this, first imagine a single-layer film on a substrate in air, as is pictured in Figure 2.4 [39]. The index of refraction of the air is labeled as n_1, that of the film as n_2, and that of the substrate as $\widetilde{n_3} = n_3 + ik_3$. A polarized beam of light enters this film from air in Figure 2.4 at an angle ϕ_1. As this beam of light encounters the surface of the film some of it is refracted according to Snell's law [35–37, 39],

$$n_1 \sin\phi_1 = n_2 \sin\phi_2. \tag{2.5}$$

Part of the beam of light refracts at an angle ϕ_2, but part of it also reflects from the surface at an angle ϕ_1. The light within the film which encounters the substrate refracts yet further at an angle ϕ_3, and also reflects at an angle ϕ_2.

The Fresnel equations for transmission and reflection govern what fraction of the light is transmitted and reflected from an interface between two media like those in Figure 2.4 [35–37, 39]. For the interface in between air and the film of Figure 2.4 (medium 1 to medium 2), the Fresnel equations take the following form [35–37, 39],

$$r_{p12} = \frac{\widetilde{n_2}\cos\phi_1 - \widetilde{n_1}\cos\phi_2}{\widetilde{n_2}\cos\phi_1 + \widetilde{n_1}\cos\phi_2}, \tag{2.6}$$

$$r_{s12} = \frac{\widetilde{n_1}\cos\phi_1 - \widetilde{n_2}\cos\phi_2}{\widetilde{n_1}\cos\phi_1 + \widetilde{n_2}\cos\phi_2}, \tag{2.7}$$

$$t_{p12} = \frac{2\widetilde{n_1}\cos\phi_1}{\widetilde{n_1}\cos\phi_2 + \widetilde{n_2}\cos\phi_1}, \tag{2.8}$$

$$t_{s12} = \frac{2\widetilde{n_1}\cos\phi_1}{\widetilde{n_1}\cos\phi_1 + \widetilde{n_2}\cos\phi_2}. \tag{2.9}$$

For the interface between the film and the substrate (2,3 interface in Figure 2.4), the same set of Fresnel coefficients apply, but with each index advanced by 1. After multiple reflections and refractions the light will reflect back into the air, giving the

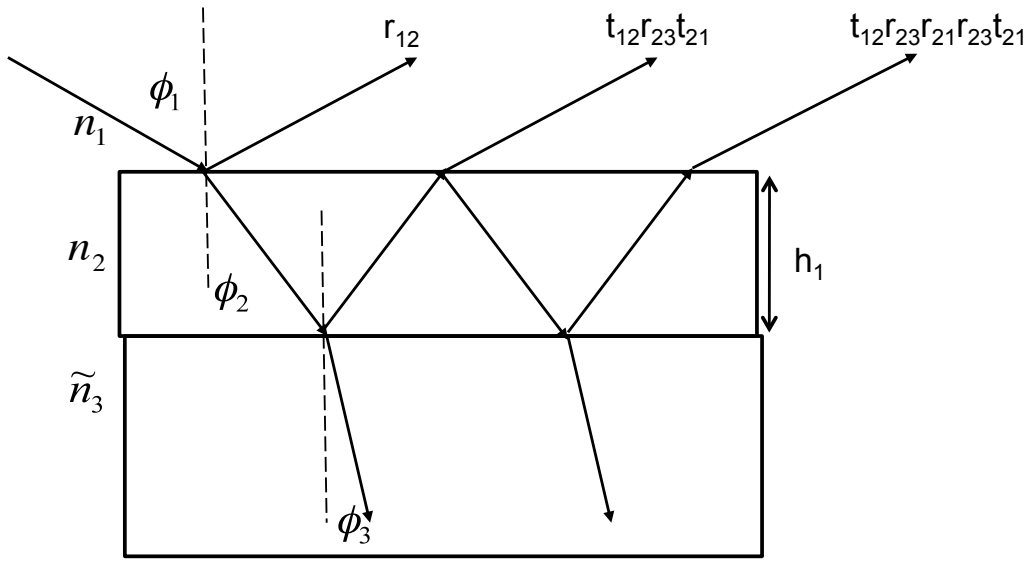

Figure 2.4: This figure shows how light transmits from air (n_1) through a single layer film (with film thickness h_1 and index of refraction n_2) and a substrate of complex index of refraction $\widetilde{n}_3$, where $\widetilde{n}_3 = n_3 + ik_3$ [39]. The substrate is considered to be infinitely thick compared to the penetration depth of the incoming beam of light. The angles of incidence and refraction are labeled (ϕ_1, ϕ_2, ϕ_3). The incoming ray of light reflects and refracts through the film and substrate multiple times. The relevant Fresnel reflection and transmission coefficients (r_{12}, t_{12}, etc.) are also written above each reflected ray.

arrows coming out of the film in Figure 2.4 [39]. The optical path difference between these adjacent reflected beams of light is related to a phase difference β. The phase of the light is shifted by an amount [39],

$$\beta = \frac{2\pi}{\lambda} n_2 h_1 \cos\phi_1, \tag{2.10}$$

where λ is the wavelength of the light in a vacuum, and the other terms have been described before [36, 37, 39]. It is known that the incident electric field E_0 is reflected and transmitted many times from the film, so the electric field in each of these cases is given by the phase difference and the Fresnel reflection and transmission coefficients, seen visually in Figure 2.4 [39]. Each component, E_1, E_2, E_3, and so on has a given form in terms of the initial electric field E_0 [35, 42],

$$E_1 = r_{12} E_0, \tag{2.11}$$

$$E_2 = t_{12} r_{23} t_{21} e^{-i\beta} E_0, \tag{2.12}$$

$$E_3 = t_{12} r_{23} r_{21} r_{23} t_{21} e^{-2i\beta} E_0. \tag{2.13}$$

Remember that each component E_1, E_2, E_3, etc. has both a p and an s component associated with it. The total Fresnel reflection coefficient resulting from all the reflected beams of light (r_{tot}) in Figure 2.4 will be [39, 42],

$$r_{tot} = r_{12} + t_{12} t_{21} r_{23} e^{-2i\beta} \left[1 + r_{21} r_{23} e^{-2i\beta} + \left(r_{21} r_{23} e^{-2i\beta}\right)^2 + ...\right]. \tag{2.14}$$

This equation can be simplified by letting $x = r_{12} r_{23} e^{-2i\beta}$ so that the total reflection coefficient r_{tot} becomes [39],

$$r_{tot} = r_{12} + t_{12} t_{21} r_{23} e^{-2i\beta} \left[1 + x + x^2 + ...\right]. \tag{2.15}$$

The series expansion,

$$\frac{1}{1-x} = 1 + x + x^2 + x^3 + ... \tag{2.16}$$

gives,

$$r_{tot} = r_{12} + \frac{t_{12}t_{21}r_{23}e^{-2i\beta}}{1 - r_{12}r_{23}e^{-2i\beta}}. \tag{2.17}$$

This relation is much more compact than the first expression.

Two relations between the Fresnel coefficients exist to help simplify Eq. (2.17) further [35]:

$$r_{12} = -r_{21}, \tag{2.18}$$

$$t_{12}t_{21} = 1 - r_{12}^2. \tag{2.19}$$

By using these relations and rearranging, the final desired form of r_{tot} is obtained [36, 37, 39, 42]:

$$r_{tot} = r_{12} + \frac{(1 - r_{12}^2)\, r_{23}e^{-2i\beta}}{1 + r_{12}r_{23}e^{-2i\beta}}, \tag{2.20}$$

$$r_{tot} = \frac{r_{12}\left(1 + r_{12}r_{23}e^{-2i\beta}\right)}{1 + r_{12}r_{23}e^{-2i\beta}} + \frac{(1 - r_{12}^2)\, r_{23}e^{-2i\beta}}{1 + r_{12}r_{23}e^{-2i\beta}}, \tag{2.21}$$

$$r_{tot} = \frac{r_{12} + r_{12}^2 r_{23}e^{-2i\beta} + r_{23}e^{-2i\beta} - r_{12}^2 r_{23}e^{-2i\beta}}{1 + r_{12}r_{23}e^{-2i\beta}}, \tag{2.22}$$

$$r_{tot} = \frac{r_{12} + r_{23}e^{-2i\beta}}{1 + r_{12}r_{23}e^{-2i\beta}}. \tag{2.23}$$

This total reflection coefficient (Eq. (2.23)) is used to relate the total reflected electric field $E_{reflected}$ to the total incident electric field E_0,

$$E_{reflected} = r_{tot}E_0. \tag{2.24}$$

Remember that the total reflection coefficient has two components p and s,

$$r_{tot}^p = \frac{r_{12}^p + r_{23}^p e^{-2i\beta}}{1 + r_{12}^p r_{23}^p e^{-2i\beta}}, \tag{2.25}$$

$$r_{tot}^{s} = \frac{r_{12}^{s} + r_{23}^{s} e^{-2i\beta}}{1 + r_{12}^{s} r_{23}^{s} e^{-2i\beta}}. \tag{2.26}$$

In this final form, these total Fresnel reflection coefficients, whose β constants contain information on film thickness h and index of refraction n of the films, can be used to obtain ψ and Δ [36, 37, 39, 42],

$$\frac{r_p^{tot}}{r_s^{tot}} = \rho = \tan\psi e^{i\Delta}. \tag{2.27}$$

The terms ψ and Δ can also be written as a function of r_p^{tot}, r_s^{tot}, and ρ,

$$\frac{|r_p^{tot}|}{|r_s^{tot}|} = \tan\psi, \tag{2.28}$$

$$\Delta = \tan^{-1}\left(\frac{Im[\rho]}{Re[\rho]}\right). \tag{2.29}$$

where $|r_p^{tot}|$ and $|r_s^{tot}|$ are the magnitudes of the total Fresnel coefficients polarized in the directions parallel and perpendicular to the plane of incidence [36].

For a multilayer film, the formula for the total Fresnel reflection coefficient (Eq. (2.23)) can be used repeatedly [42]. Imagine now that there is a bilayer film on a substrate in air, as pictured in Figure 2.5. The top film has a film thickness of h_1 and an index of refraction n_2, while the bottom film has a film thickness of h_2 and an index of refraction of n_3. This lower film can also represent the layer of native oxide atop the silicon substrate. Recall the formula for the total Fresnel reflection coefficient [39, 42]:

$$r_{tot} = \frac{r_{12} + r_{23} e^{-2i\beta_2}}{1 + r_{12} r_{23} e^{-2i\beta_2}}, \tag{2.30}$$

where β_2 is the optical phase difference of the top film in the bilayer stack [42],

$$\beta_2 = \frac{2\pi}{\lambda} n_2 h_1 \cos\phi_2. \tag{2.31}$$

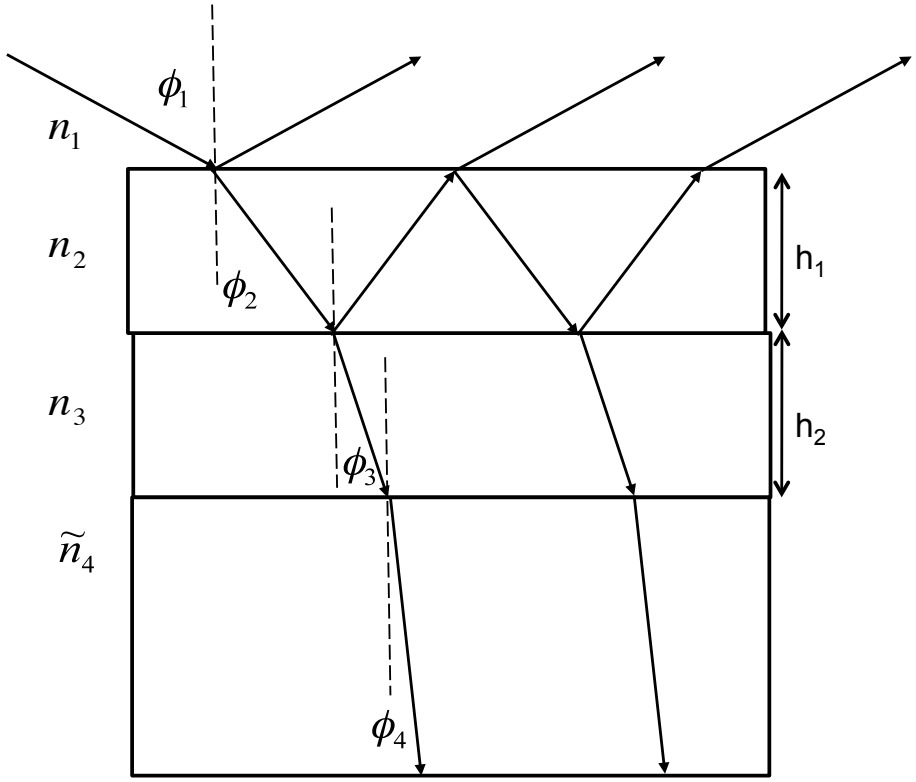

Figure 2.5: This figure shows how light reflects and refracts from a bilayer film of thicknesses h_1 and h_2 on a substrate sitting in air. The reflected arrows from the 3,4 interface are not shown for clarity of viewing the figure.

Replace r_{23} with r_{23}^{tot}, which is the total Fresnel reflection coefficient of the second film with film thickness h_2 [42],

$$r_{23}^{tot} = \frac{r_{23} + r_{34}e^{-2i\beta_3}}{1 + r_{23}r_{34}e^{-2i\beta_3}}, \tag{2.32}$$

where β_3 is the optical phase difference for the second film [42],

$$\beta_3 = \frac{2\pi}{\lambda} n_3 h_2 \cos\phi_3. \tag{2.33}$$

The total Fresnel reflection coefficient for the bilayer film will then be [42],

$$r_{tot} = \frac{r_{12} + r_{23}^{tot}e^{-2i\beta_2}}{1 + r_{12}r_{23}^{tot}e^{-2i\beta_2}}. \tag{2.34}$$

In general, this process can be repeated indefinitely for the number of films required [36, 42]. Figure 2.6 depicts computer generated curves of ψ vs. λ and Δ vs. λ for a hypothetical 500 nm PS film supported on native silicon with the native oxide intact. The MATLAB program which generated these curves is in the Appendix of this thesis. Comparison data is shown for a polystyrene film 500 nm thick supported on silicon with a native oxide layer generated using WVase32. The match between the data generated using WVase32 and MATLAB is excellent, showing that the formulas above produce values correlated to what the ellipsometer measures.

2.2.3 Modeling and Fitting Ellipsometry Data

The supported polystyrene film is modeled as a three-layer film composed of a silicon support, a native silicon oxide layer, and the polymer film. A schematic of this model is depicted in Figure 2.7. The dependence of index of refraction on wavelength is known for silicon and the native oxide layer, seen in Figure 2.4, and the thicknesses of the substrate layers are set to 2 nm for native oxide and 1 mm for silicon (1 mm

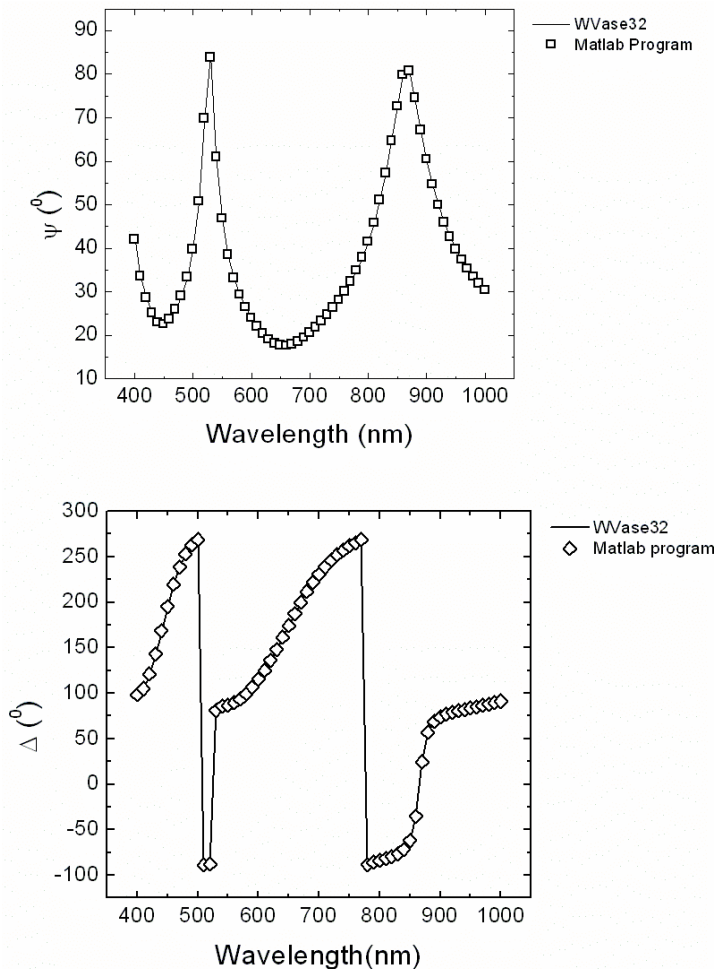

Figure 2.6: These figures depict curves of ψ and Δ dependent on wavelength λ of a hypothetical 500 nm polystyrene film supported on a silicon layer with native oxide intact generated by the MATLAB program listed in the Appendix and WVase32, software which came with the ellipsometer and is designed to analyze the resulting data. The match between the two programs is excellent.

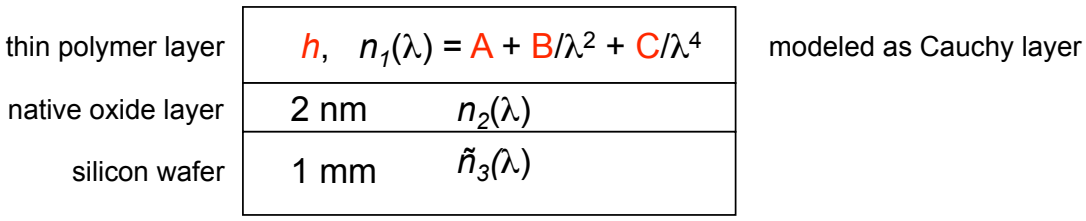

Figure 2.7: This figure shows how WVase32 models the supported polymer film. The two bottom layers represent the silicon wafer with its native oxide. The Cauchy model is used to estimate the index of refraction of the top polymer layer [36]. The film thickness h and the three constants A, B, C are inserted into WVase32, and adjusted iteratively until a best fit is found using a Levenberg-Marquandt algorithm [36].

is infinitely thick compared to the penetration depth of the light). To determine the index of refraction of the polymer layer, however, a Cauchy model is applied [36, 37],

$$n(\lambda) = A + \frac{B}{\lambda^2} + \frac{C}{\lambda^4}, \tag{2.35}$$

where λ is the wavelength of light and A, B, and C are constants [36, 37]. Guesses are inserted for parameters of film thickness h, constants A, B, and C, and the fit is adjusted iteratively using a Levenberg-Marquandt algorithm until a global minimum is reached [36]. The resulting generated curves of ψ vs. λ and Δ vs. λ should match the measured data. From these curves, values of film thickness h and index of refraction n are produced.

2.3 Glass Transition Temperature Measurements

The ellipsometer is used to track the changes in film thickness and index of refraction with temperature in order to determine the glass transition temperature of bulk polystyrene films. To measure T_g, a PS film is heated above its glass transition temperature to a temperature of 150 °C for 25 minutes to remove its thermal history, then cooled slowly at a rate of 1 °C/minute. During cooling, measurements of film

thickness and index of refraction are recorded. The resulting data are plotted in two graphs: Figure 2.8 (A) shows the dependence of film thickness on temperature, and Figure 2.8 (B) shows the dependence of index of refraction on temperature for a single representative PS film supported on silicon. The intersection of the fits to the linear portions of the data in Figure 2.8 (A) gives the glass transition temperature, as well as the intersection of similar lines in Figure 2.8 (B). From an average of five different runs, the glass transition temperature of polystyrene was measured to be (97 ± 2) °C. These linear fits also measure the change in film thickness with temperature and index of refraction on temperature for supported polystyrene films. This information is used later in order to determine the physical aging rates of the polymer films. Values of $(dh/dT)_{glassy}$ and $(dn/dT)_{glassy}$ were measured over a temperature range of T = 37 °C to T = 90 °C. Values of $(dh/dT)_{liquid}$ and $(dn/dT)_{liquid}$ were measured over the temperature range of 105 °C to 140 °C. The measured values are listed in Table 2.1.

Table 2.1: Slopes of Film Thickness and Index of Refraction Above and Below T_g

Temperature Range (°C)	dh/dT (nm/°C)	dn/dT (/°C)
37 °C to 90 °C	0.44 ± 0.02	(-1.14 ± 0.05) x 10^{-4}
105 °C to 140 °C	1.53 ± 0.04	(-3.80 ± 0.11) x 10^{-4}

2.4 Experimental Procedure for Physical Aging Measurements

The ellipsometer is used to characterize the physical aging of polystyrene films by tracking changes in the film thickness and index of refraction over time. The experiment begins by heating the film in an oven equilibrated at (130 ± 3) °C for

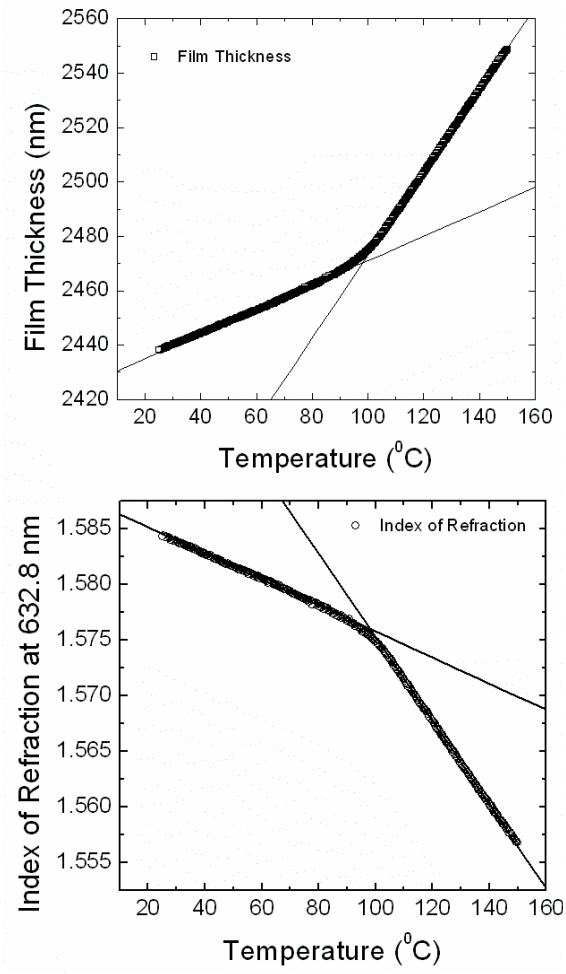

Figure 2.8: (Top) This figure shows the dependence of film thickness on temperature for a supported PS film being cooled slowly at 1 °C/min. The glass transition temperature is located near the point in the graph where the slope changes. It is determined by first fitting lines to the linear portions of the data. The intersection of these two lines gives the glass transition temperature. (Bottom) This figure shows the dependence of the index of refraction on temperature for the same PS film as at the top being cooled slowly at 1 °C/min. Again, T_g can be extracted by locating the intersection of two lines fit to the linear portions of the data.

(30 ± 5) minutes, to remove any thermal history of the film. The film is then removed from the oven and quenched on a room temperature aluminum block for one minute. The film is taken to the ellipsometer, aligned on the hot stage that has been equilibrated to the aging temperature for 30 minutes prior to the start of the physical aging measurement, and the aging run begins. Zero time is defined as the point where the polymer goes through the glass transition upon quenching. For aging runs lasting 24 hours, the values of ψ vs. λ and Δ vs. λ are measured every five minutes and averaged over a period of 30 seconds. For aging runs lasting 360 minutes, ψ vs. λ and Δ vs. λ are measured every two minutes, but still averaged over a period of 30 seconds. At aging temperatures above 85 °C, polystyrene could oxidize with the air, changing the physical aging rate [43]. To prevent this, a dry nitrogen gas flow is gently applied across the surface of the film. At aging temperatures of 50 °C and below, a liquid nitrogen feed is applied to stabilize the aging temperature. Also, ultraviolet radiation could adversely affect polystyrene, causing differences in physical aging rates [43]. For this reason, the D2 lamp on the ellipsometer is not used during these physical aging experiments.

2.4.1 Comparison of Physical Aging Procedure to Existing Literature

The closest aging experiment existing in the literature to that used in this thesis is the physical aging experiment of Huang and Paul using ellipsometry [2]. There are two relevant differences between their work and the work presented here. Their films are quenched in a free-standing state [2], while the films used in this thesis are quenched in a supported state. The second difference concerns the physical aging time and measurement frequency. They take one aging measurement every few days over the space of a year, taking the film on and off of the ellipsometer between each measurement [2]. The measurements in this thesis take place every few minutes over

24 hours, continuously, taking advantage of the high relative accuracy of ellipsometry measurements. Once the film is placed on the hot stage of the ellipsometer, it does not leave until the physical aging experiment is complete.

The concept of using ellipsometry to study physical aging to track changes in film thickness over time is not new. Work by Richardson, López-García, Sferrazza, and Keddie have already provided a basis for using the ellipsometer as a means to detect changes in the film thickness of PMMA films during solvent evaporation [3]. Their results indicate that the change in film thickness due to solvent evaporation is roughly 1000 times greater than the change in film thickness of an aging film that has already had all solvent removed [3]. However, the tiny relative changes in volume occurring in the film with all solvent removed is still able to be detected by the ellipsometer [3]. Because these tiny relative film thickness changes can be detected using ellipsometry [3], the new ellipsometry method in this thesis should also be able to detect the changes in film thickness.

Chapter 3

Physical Aging Results

3.1 Physical Aging Results

Ellipsometry was used to detect changes in film thickness and index of refraction of supported polystyrene films during physical aging using the method developed in Section 2.4. Representative changes in the film thickness and index of refraction, for a 2.58 μm supported PS film aged for 24 hours on native silicon, are shown in Figures 3.1 (A) and (B). Figures 3.1 (A) and (B) represent the changes in film thickness and index of refraction of the PS film when it was aged at 75 °C (348 K) compared to when it was held at a temperature of 105 °C (378 K), above its measured glass transition temperature of (97 ± 2) °C. Changes in the film thickness and index of refraction of the film at 105 °C are very small (less than 0.02% [10]) compared with the changes in film thickness and index of refraction of the PS film aged at 75 °C. From Figures 3.1 (A) and (B) it can be determined that the changes in film thickness and index of refraction measured at temperatures below T_g are due to physical aging.

The stability of measurements of film thickness and index of refraction are important parameters to know in order to determine the precision of the aging measurements. In order to test the precision of the measurements taken by the ellipsometer, a silicon oxide standard calibration film 1000 nm thick supported on silicon was held

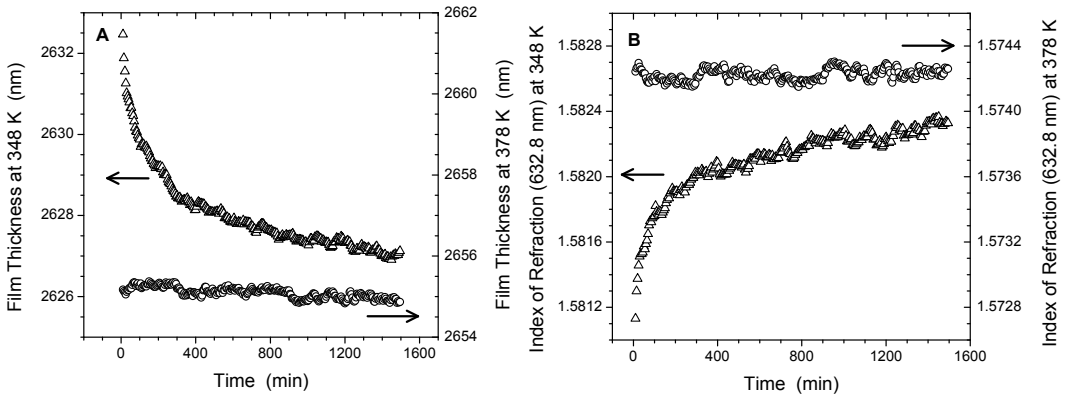

Figure 3.1: Both of these figures show physical aging data measured by ellipsometry over 24 hours for a representative 2.58 μm thick PS film supported on silicon. (A) This figure shows the change in film thickness over time of a supported polystyrene film aged at 75 °C (348 K) (upwards-pointing triangles) and the same film held at a temperature of 105 °C (378 K) (circles). At 105 °C, there is no significant change in film thickness over 24 hours compared to the changes in film thickness at 75 °C. (B) This figure shows the changes in index of refraction measured with light of wavelength 623.8 nm (to correspond with HeNe laser ellipsometer measurements [36]) plotted against time of the same supported PS film aged at 75 °C (348 K) (upwards-pointing triangles) and the same film held at a temperature of 105 °C (378 K) (circles). The changes in the index of refraction over the aging time are much larger when the film is aged at 75 °C than when it is aged at 105 °C. Both of these figures provide evidence that the changes in film thickness and index of refraction measured over the aging time at temperatures below T_g are due to physical aging.

at 75 °C (348 K) following the same protocol developed in Section 2.4 of this thesis for a supported PS film. Using this protocol, the silicon oxide film acts like a model supported PS film, with a similar film thickness and index of refraction. Because the silicon oxide film is never heated above its glass transition temperature (∼1000 °C [44]), it is anticipated to show little or no change in thickness or index of refraction during the time of the measurement. The results of this experiment are shown in Figures 3.2 (A) and (B), which display the change in film thickness and index of refraction of the 2.58 μm PS film held at a temperature of 105 °C (378 K) (seen earlier in Figures 3.1 (A) and (B)) compared to the same parameters for the aging of the silicon oxide film held at 75 °C (348 K). The variation of the film thick-

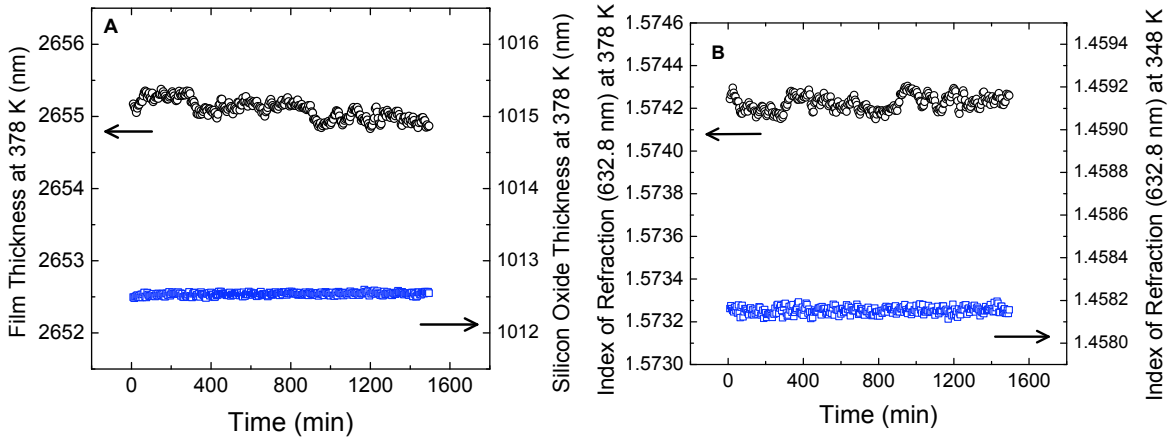

Figure 3.2: (A) This figure shows the change in film thickness over time of a representative 2.58 μm supported PS film (circles) held at a temperature of 105 °C (378 K) over 24 hours and a supported ∼1000 nm silicon oxide standard calibration layer (squares) held at a temperature of 75 °C over 24 hours. (B) This figure shows the change in index of refraction of a representative 2.58 μm PS supported film (circles) held at a temperature of 105 °C and a supported ∼1000 nm silicon oxide film (squares) held at a temperature of 75 °C over 24 hours. The silicon oxide film was measured using the same protocol as if it were a PS film being aged at 75 °C, using the method in Section 2.4, except that it never is heated above its glass transition temperature (∼1000 °C [44]).

ness and index of refraction of the silicon oxide film over time is even smaller than the variation in film thickness and index of refraction of the PS sample over time held at a temperature of 105 °C. The silicon oxide run acts as a baseline to the ellipsometry measurements: any changes detected in the film thickness and index of refraction of a PS film over time is not attributable to changes in the substrate thickness, temperature fluctuations, vibrations of the table on which the ellipsometer rests, or changes in the ventilation system of the room. The physical aging method developed in Section 2.4 successfully characterizes changes in height and index of refraction using ellipsometry.

One of the central themes of physical aging is the ability to erase previous physical aging of the material by heating it above its glass transition temperature long enough

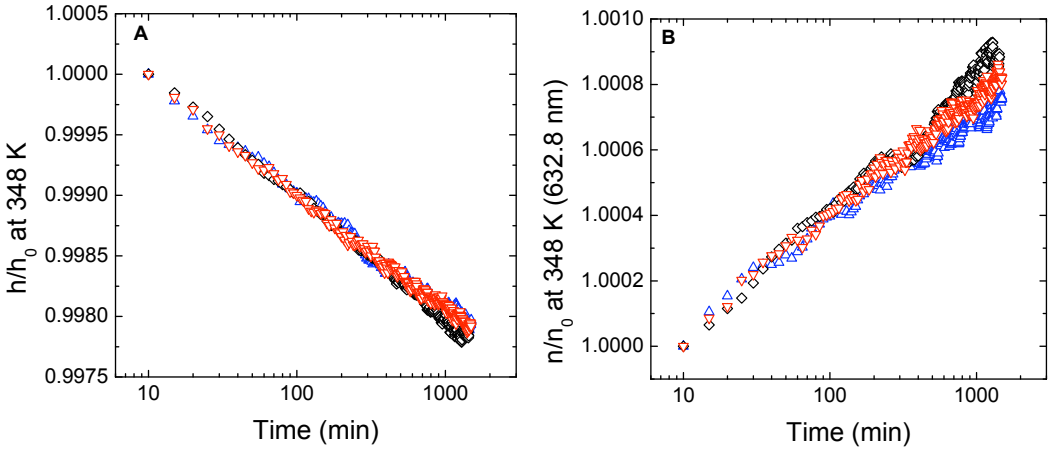

Figure 3.3: These figures show changes in the normalized film thickness and index of refraction measured using ellipsometry for two representative 2.58 μm PS films supported on silicon aged at 75 °C for 24 hours. (A) This graph shows film thickness normalized by the film thickness measured at 10 minutes into the aging run (h_0) plotted against time of a supported PS film heated and quenched once below T_g (upwards-pointing triangles) and heated above T_g and quenched a second time below T_g (diamonds). The normalized film thickness of a separate PS film is also displayed (downwards-pointing triangles). (B) This graph shows the index of refraction normalized by the index of refraction measured at 10 minutes into the aging run (n_0) plotted against time measured with light of wavelength 632.8 nm of the same PS films as part (A).

to remove its thermal history [7, 9, 20]. To have an objective comparison between samples, however, a normalization factor will have to be used. This normalization factor means that physical aging rates calculated at different film thicknesses or different aging temperatures can all be compared to one another. Figure 3.3 (A) shows the film thickness normalized by the initial film thickness taken at 10 minutes into the aging run, h_0, collected for a 2.58 μm supported PS film on native silicon when aged at 75 °C and then placed aside for one year, heated again to (130 ± 3) °C for (30 ± 5) minutes, quenched, and aged again for 24 hours. The reproducibility of the physical aging measurements also needs to be demonstrated. Normalized film thickness measurements for a separate PS film are also displayed, demonstrating reproducibility. Figure 3.3 (B) is the same data collected from the same PS films aged at the same aging temperature, only displaying the index of refraction normalized by its value at 10 minutes into the aging run, n_0. Again, both the erasure of physical aging and the reproducibility of the measurements are demonstrated in this figure.

Zero aging time is defined as when the polymer film, equilibrated in an equilibrium liquid state, goes through Tg upon quenching. This zero aging time is not identical to $t = 0$ as recorded on the ellipsometer because the oven and the ellipsometer are in different rooms. Approximately two minutes are required to quench the film, transfer it to the ellipsometer, align it, and start recording changes in film thickness and index of refraction. During these two minutes, the polymer film experiences little to no physical aging because it is at room temperature. The first data point at which the physical aging rate is determined starts not at $t = 0$, but at $t = 10$ minutes as recorded on the ellipsometer (see Section 3.2). This is because the film requires approximately 10 minutes to thermally equilibrate and bring the aging rate up to the value it has at a given aging temperature. Technically, the time before well-defined aging begins is approximately 12 minutes, not 10 minutes. However, during these 12 minutes, the physical aging rate is ill-defined and significantly less than the

physical aging rate during the measurement. We artificially define this 12 minute period of time as an aging time of "10 minutes. Defining this time to be 12 minutes instead of 10 minutes does not alter the calculations of physical aging rate (as defined in Section 3.2) beyond more than one standard deviation in the average value of β.

3.2 Determination of Physical Aging Rate β

Table 3.1: Table of Physical Aging Rate Formulas

Method 1	$\beta_1 = -\frac{1}{h_\infty}\left(\frac{\partial h}{\partial \log t}\right)_{P,T}$
Method 2	$\beta_2 = -\frac{1}{h_0}\left(\frac{\partial h}{\partial \log t}\right)_{P,T}$
Method 3	$\beta_3 = \frac{1}{L_\infty}\left(\frac{\partial L}{\partial \log t}\right)_{P,T}$
Method 4	$\beta_4 = \left(\frac{\partial n}{\partial \log t}\right)_{P,T}\left(\frac{\partial n}{\partial T}\right)^{-1}_{P,t}\alpha_g$

A study of the research literature reveals four different methods by which the physical aging rate β can be calculated. All four of these methods use the slope of fits to the analyzed data to calculate the physical aging rate. The first method is a one-dimensional modification of the original method used by Struik [6] (Method 1, Table 3.1). The term h_∞ is the theoretical equilibrium film thickness obtained if the film was cooled infinitely slowly. The second method is a modification of the first, but with the use of h_0 instead of h_∞. The idea to normalize the data by the initial value of the measured parameter (in their case, intensity; in our case, film thickness) at 10 minutes into the aging run h_0 was proposed by Royal and Torkelson (Method 2, Table 3.1) [34]. At most, the difference in between h_0 and h_∞ is a few nanometers, so the physical aging rates calculated from Method 2 should be very similar to those of Method 1. The third method takes advantage of the optical constants of the film by

using the Lorentz-Lorenz equation (Method 3, Table 3.1), which relates the density of the polymer film to the index of refraction [2],

$$L = \frac{n^2 - 1}{n^2 + 2} = C\rho, \tag{3.1}$$

where C is a constant defined by,

$$C = \frac{N_A \sum n_i \alpha_i}{3 M_0 \epsilon_0}, \tag{3.2}$$

where ρ is the density, N_A is Avogadro's Number, α_i is the polarizability of a bond, n_i is the number of such bonds, M_0 is the molecular weight of the repeat unit, and ϵ_0 is the permittivity of free space [23, 24, 45, 46]. The method was first used by Robertson and Wilkes [45], and variations on this method have since been adapted for use by Huang and Paul [2, 19, 22–25]. The fourth method (Method 4, Table 3.1) uses not only the dependence of the index of refraction on logarithmic time, but also the dependence of the index of refraction and film thickness on temperature in the glassy state [45]. This is a second method evaluated by Robertson and Wilkes [45]. The values of dn/dT and dh/dT were determined by measuring the change in film thickness and index of refraction with temperature in the glassy and liquid states as discussed in Section 2.3 (Table 2.1). Each one of these four analysis techniques (Table 3.1) were used to extract physical aging rates from the changes in film thickness and index of refraction measured over time from the PS films. All fits to the physical aging data are performed by constraining the linear fit to intercept the first data point at 10 minutes into the aging run. By definition, physical aging begins at this point, thus characterizing the physical aging rate as the total amount of physical aging (rise) over the total aging time (run), similar to work by Rittigstein and Torkelson [33] and Huang and Paul [23].

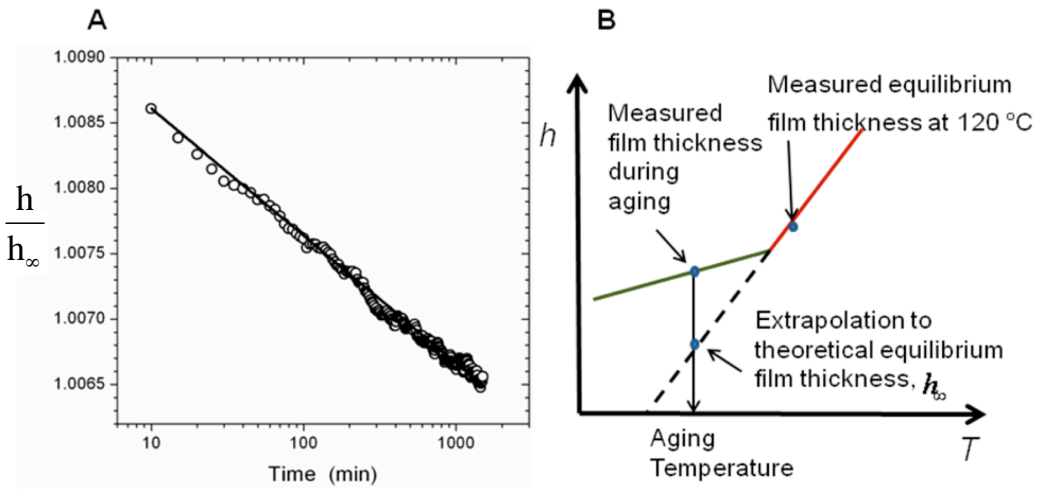

Figure 3.4: (A) This figure shows the film thickness normalized by the theoretical equilibrium film thickness (h/h_∞) plotted against logarithmic time of a representative 2.58 μm PS film supported on native oxide on silicon aged at 75 °C for 24 hours. The slope of a line fit to this data produces the physical aging rate (Method 1, Table 3.1). (B) This schematic shows how the theoretical equilibrium film thickness is estimated. First, a measurement of the height of the PS film at 120 °C is taken. This data point can be combined with the slope of the equilibrium liquid line in order to extend the equilibrium liquid line below T_g. The point along the extrapolated line (dashed line in (B)) at the aging temperature produces an estimate of the theoretical equilibrium film thickness h_∞.

3.2.1 Method 1 Film Thickness Normalized at h_∞

The first method by which the physical aging rate is determined is a one-dimensional analog of the original method used by Struik [6] (Method 1, Table 3.1). While the original method applies to volume dilatometry, length dilatometry also uses a one-dimensional application of the method [21]. Normalizing by h_∞ has been used more recently in ellipsometry measurements by Richardson, López-García, Sferrazza, and Keddie [3]. Figure 3.4 (A) plots the change in film thickness of a 2.58 μm PS film normalized by the estimated equilibrium film thickness h_∞ plotted against logarithmic time supported on native silicon aged at 75 °C (378 K) for 24 hours. The slope of this linear fit provides the physical aging rate by Method 1, Table 3.1.

What is the best way to estimate the equilibrium film thickness h_∞?

The most common way of estimating the theoretical equilibrium film thickness h_∞ is to use a linear extrapolation of the equilibrium liquid line [1, 7, 19, 47–49]. This is the linear dashed line in Figure 3.4 (B), which shows the expected glassy and equilibrium liquid states of the film thickness h plotted against temperature T. For the physical aging experiments presented in this thesis, h_∞ is calculated by measuring the film thickness at 120 °C, directly on the equilibrium liquid line, as shown in Figure 3.4 (B). The film thickness at this temperature above T_g is measured by allowing the film to equilibrate on the hot stage for 10 minutes and then measuring its film thickness every 10 seconds for five minutes. The average of the film thickness and index of refraction over this time gives the film thickness h_{120} of the PS film at 120 °C. The combination of h_{120} and the slope of the equilibrium liquid line provides the necessary information to extend the line below T_g (dashed line in Figure 3.4 (B)). The point along this line at the given aging temperature defines the theoretical equilibrium film thickness h_∞. A similar extrapolation is performed to calculate the value of n_∞, which is necessary to calculate the physical aging rates using the Lorentz-Lorenz equation (Method 3) and the index of refraction (Method 4, Table 3.1).

However, two other methods exist in the literature besides the linear extrapolation to estimate the theoretical equilibrium film thickness. Each of these methods is depicted in Figure 3.5. The first method, the linear extrapolation of the previous paragraph, is represented by the large dashes [1, 7, 19, 47–49]. The second method utilizes the Tait equation, which concerns the "compressibility of liquids"(short dashes) [18, 50–52]. For PS, the volume "at zero pressure" depends on the aging temperature by $V(0,T) = 0.9287 \exp\left[5.131 \times 10^{-4} T\right]$ [50,52] which is nearly a straight line. The third method utilizes the transition temperature T_2 (50 °C for PS [56]) of the Adam-Gibbs relation, the temperature at which "entropy extrapolates to zero" [53–55]. Above T_2, this extrapolation follows along the equilibrium

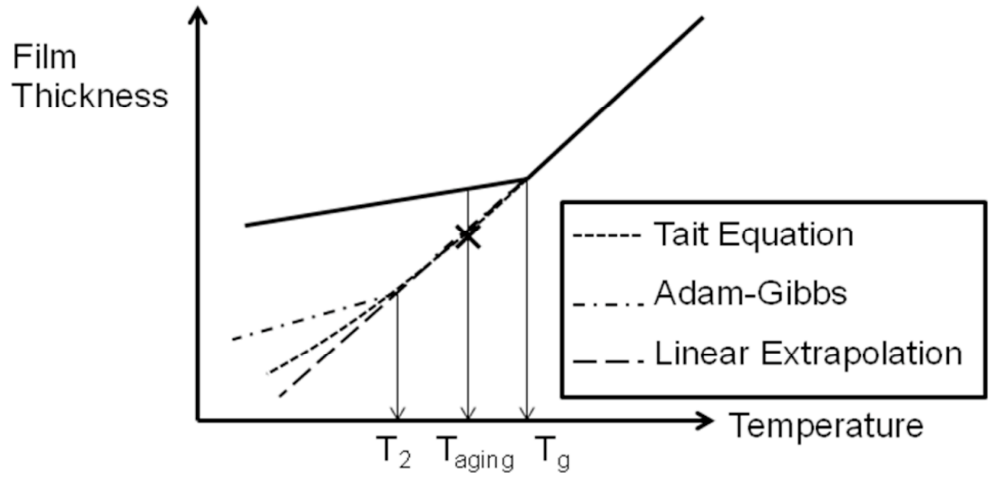

Figure 3.5: This schematic depicts the most common way to estimate the theoretical equilibrium film thickness, the Linear Extrapolation (large dashes) [1, 7, 19, 47–49]. The equilibrium liquid line is extended below the glass transition temperature T_g to produce this graph [1, 7, 19, 47–49]. Two other methods exist within the literature to estimate the theoretical equilibrium film thickness. The second method mentioned uses the Tait equation, which was originally used to define the "compressibility of liquids" (short dashes) [18,50–52]. This curve, for PS, is of the form of an exponential function to the 10^{-4} power, almost a straight line [50, 52]. The third method uses Adam-Gibbs theory to join two straight lines together at temperature T_2 [53–55], which for PS is 50 °C [56] (dash-dots). Above T_2, this extrapolation follows along the equilibrium liquid line [53–55]. The bold **X** designates the theoretical equilibrium film thickness of a polymer film aged at T_{aging}.

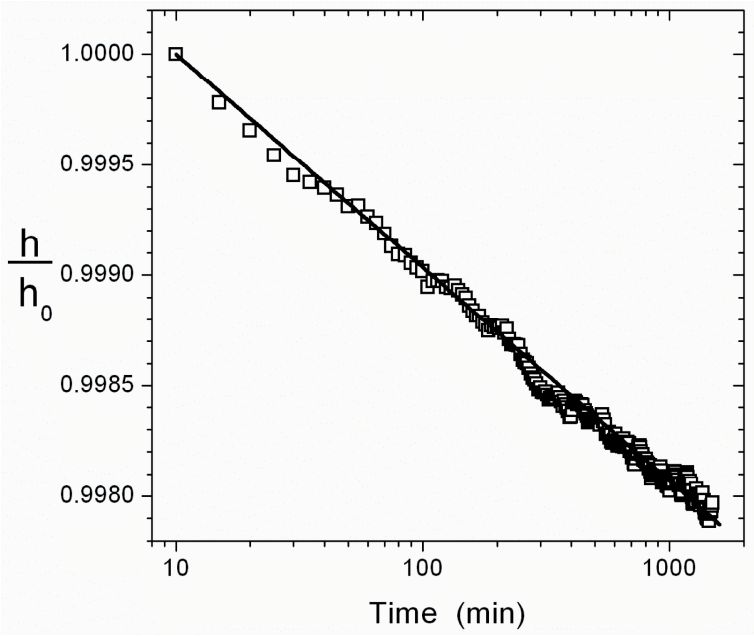

Figure 3.6: This graph shows the change in film thickness normalized by the film thickness measured at 10 minutes into the aging run h_0 plotted against logarithmic time for a representative 2.58 μm PS film supported on silicon aged at 75 °C for 24 hours. The slope fit to this data gives the physical aging rate β (Method 2, Table 3.1).

liquid line [53–55]. Considering that all three methods are *estimates* of h_∞ which at low physical aging temperatures cannot be realized on a reasonable time scale, the majority of the physical aging literature uses the linear extrapolation. Because there is no significant justification for using the other two methods, the simple linear extrapolation will be used to determine h_∞ and n_∞.

3.2.2 Method 2 Film Thickness Normalized at h_0

The second method applied to determine the physical aging rate is a modification of one used by Torkelson and coworkers for fluorescence measurements [1, 17, 29, 30, 33, 34, 57] (Method 2, Table 3.1). Instead of normalizing to the theoretical equilibrium film thickness h_∞, the film thickness is normalized to the film thickness measured at 10 minutes into the aging run h_0. Royal and Torkelson did not measure changes in

film thickness over time, but changes in fluorescence intensity over time [34]. Figure 3.6 depicts the change in film thickness of a supported 2.58 μm PS film on native silicon normalized by the film thickness at 10 minutes h_0 plotted against logarithmic time aged for 24 hours at 75 °C (378 K). The slope gives the physical aging rate.

In their fluorescence experiments, Torkelson and coworkers used the normalization F_0, (the fluorescence intensity measured 10 minutes into the aging run), instead of F_∞, (the theoretical equilibrium fluorescence intensity), to calculate the physical aging of polymer films containing fluorescent probes [17, 29–31, 34]. Suppose that they wanted to calculate F_∞, in analog to the most common method mentioned in Section 3.2.1, by extending the slope of a line of intensity vs. temperature of a polymer in the liquid state below T_g. The intensity measured from the probes, however, relies upon the hinderance in their rotation due to their surroundings. If the polymer is in a liquid state above T_g, the probes would not experience much hindrance of their motion because the segments of the polymer chain are more mobile. Without being hindered, the intensity from the probes would not change. Without a change in intensity with temperature, there is no slope to extend below T_g on a graph of intensity vs. temperature in order to calculate F_∞. Therefore, Torkelson and coworkers then chose to normalize by F_0 as a reasonable alternative.

There are two other advantages to normalizing the measured parameter to its value at 10 minutes for physical aging experiments (film thickness for the experiments in this thesis, intensity for the experiments of Torkelson and coworkers [17,29–31,34]): one, at 10 minutes into the aging time the polymer film achieved thermal equilibrium [30,34]; and two, normalizing by a reference parameter provides the ability to compare the relative changes in the measured parameter over time, regardless of film thickness or aging temperature [34]. This is the most accurate of all four methods because the value of h_0 is always available without taking separate measurements, and no large extrapolations are required to calculate this physical aging rate even at lower aging

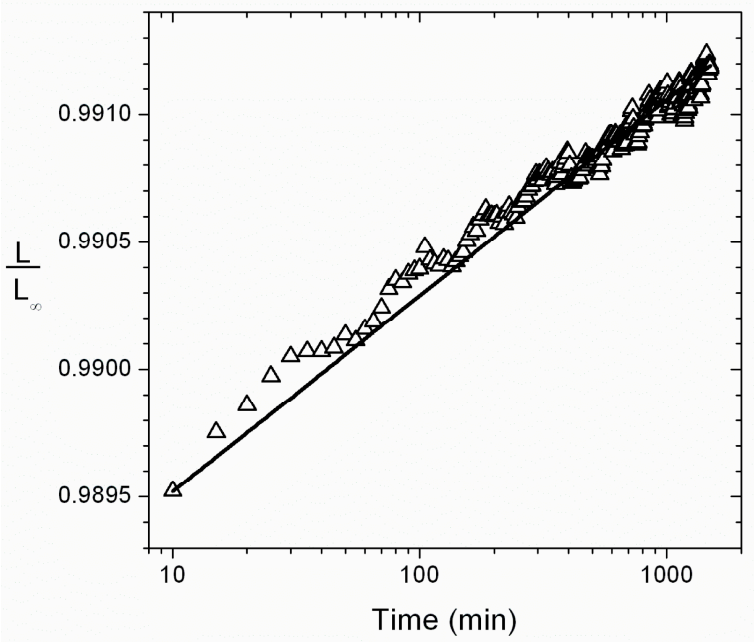

Figure 3.7: This graph shows the change in the Lorentz-Lorenz parameter L normalized by its theoretical equilibrium value L_∞ plotted against logarithmic time for a representative 2.58 μm PS film supported on native silicon aged at 75 °C for 24 hours. The slope gives the third value of the physical aging rate, β (Method 3, Table 3.1).

temperatures.

3.2.3 Method 3 Lorentz-Lorenz Equation

The third method to determine the physical aging rate uses the Lorentz-Lorenz equation (Method 3, Table 1). In Figure 3.7, the Lorentz-Lorenz parameter L normalized by its theoretical equilibrium value L_∞ is plotted against logarithmic time. The sample used to obtain this data was a 2.58 μm supported PS film on native silicon aged for 24 hours at 75 °C (378 K). Again, a slope fit to this data gives the physical aging rate. The Lorentz-Lorenz parameter is related to the density of the polymer film by Eq. (3.1). The theoretical equilibrium value of the Lorentz-Lorenz parameter L_∞ is calculated by using n_∞ in place of the index of refraction in Eq. (3.1).

The Lorentz-Lorenz equation itself arises from the relationship between the local

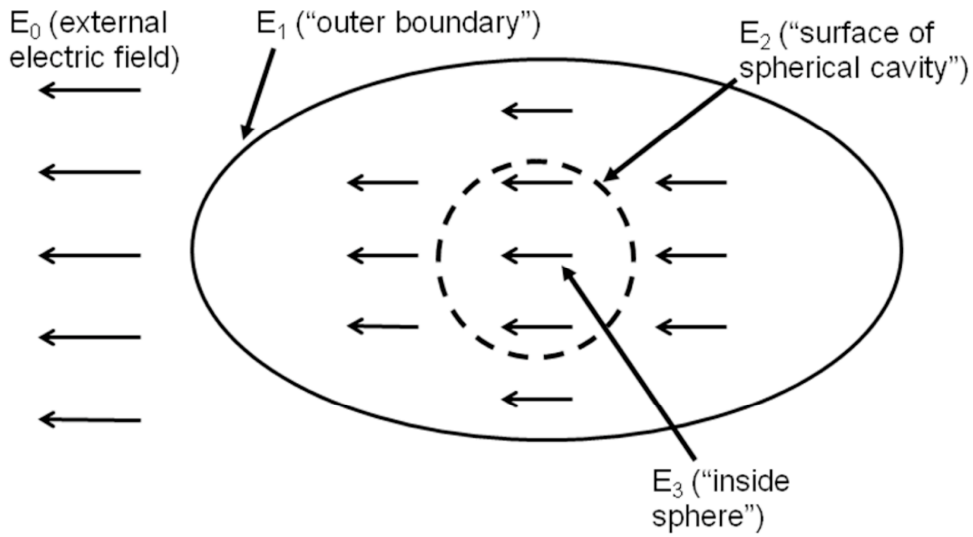

Figure 3.8: This schematic shows the different regions over which components of the local electric field E_{local} act (figure modified from ref. [58]). The arrows surrounding and inside the material are the vectors of the dipoles or the direction of the electric field [58]. A single atom is observed inside a mathematical spherical cavity carved within the body of the material [58]. E_0, comes from fixed charges external to the body [58]. E_1 is due to the uniform polarization of the material [58]. E_2 is the Lorentz cavity field, located on the surface of the spherical cavity inside the body [58]. E_3 is the field from the dipoles inside the cavity, but this field is equal to zero for a completely random lattice array, which is what is expected in an amorphous polymer [58, 59].

electric field $\vec{E}_{local}$ surrounding an atom in an array and the macroscopic electric field $\vec{E}$ [58–60]. The local electric field is composed of four pieces [58–60],

$$\vec{E}_{local} = \vec{E}_0 + \vec{E}_1 + \vec{E}_2 + \vec{E}_3. \tag{3.3}$$

Each one of these components is displayed visually in Figure 3.8. The first part of Eq. (3.3), $\vec{E}_0$, is the field produced by fixed charges external to the body [58]. The second part of this equation, $\vec{E}_1$ is the field due to the uniform polarization of the material [58]. The sum of the first two terms of this expression are equivalent to the macroscopic electric field $\vec{E}$ [58],

$$\vec{E} = \vec{E}_0 + \vec{E}_1. \tag{3.4}$$

The third term, $\vec{E}_2$, is the Lorentz cavity field, and for this case has the following form [58],

$$\vec{E}_2 = \frac{1}{3\epsilon_0}\vec{P}, \tag{3.5}$$

where $\vec{P}$ is the polarization [58]. The fourth part, $\vec{E}_3$, is equal to zero for a completely random lattice [59], which is the case for amorphous polymers. Adding all four terms together gives the following form to $\vec{E}_{local}$ [58],

$$\vec{E}_{local} = \vec{E} + \frac{1}{3\epsilon_0}\vec{P}, \tag{3.6}$$

referred to as the Lorentz relation [58].

To use this Lorentz relation (Eq. (3.6)), a relationship between the polarizability of an atom α and the dielectric constant ϵ is desired [58]. The polarization can be written as [58],

$$P = \sum_j N_j p_j = \sum_j N_j \alpha_j E_{local}(j), \tag{3.7}$$

where N_j is the concentration of j atoms and p_j is the dipole moment of the jth atom [58]. Inserting the Lorentz relation, we solve for P [58],

$$P = \sum_j N_j \alpha_j \left(E + \frac{1}{3\epsilon_0} P \right), \tag{3.8}$$

$$P \left(1 - \frac{1}{3\epsilon_0} \sum_j N_j \alpha_j \right) = E \sum_j N_j \alpha_j, \tag{3.9}$$

$$P = \frac{E \sum_j N_j \alpha_j}{1 - \frac{1}{3\epsilon_0} \sum_j N_j \alpha_j}. \tag{3.10}$$

Knowing that the dielectric susceptibility $\chi = P/(\epsilon_0 E)$, the following can be achieved [58]:

$$\chi = \frac{\frac{1}{\epsilon_0} \sum_j N_j \alpha_j}{1 - \frac{1}{3\epsilon_0} \sum_j N_j \alpha_j}. \tag{3.11}$$

Rearranging Eq. (3.11) and substituting in the relationship between ϵ and χ ($\epsilon = 1 + \chi$) gives the Clausius-Mossotti relation [58]. Starting with,

$$\chi \left(1 - \frac{1}{\epsilon_0} \sum_j N_j \alpha_j \right) = \frac{3}{3\epsilon_0} \sum_j N_j \alpha_j, \tag{3.12}$$

move all terms containing the summation over to the right-hand side and combine,

$$\chi = \chi \left(\frac{3}{3\epsilon_0} \sum_j N_j \alpha_j \right) + \frac{3}{3\epsilon_0} \sum_j N_j \alpha_j, \tag{3.13}$$

$$\chi = (\chi + 3) \left(\frac{1}{3\epsilon_0} \sum_j N_j \alpha_j \right). \tag{3.14}$$

To write in terms of the dielectric constant ϵ,

$$\chi + 1 - 1 = (\chi + 1 + 2)\left(\frac{1}{3\epsilon_0}\sum_j N_j\alpha_j\right), \tag{3.15}$$

gives,

$$\epsilon - 1 = (\epsilon + 2)\left(\frac{1}{3\epsilon_0}\sum_j N_j\alpha_j\right), \tag{3.16}$$

$$\frac{\epsilon - 1}{\epsilon + 2} = \frac{1}{3\epsilon_0}\sum_j N_j\alpha_j. \tag{3.17}$$

In this form, the equation is known as the Clausius-Mossotti relation [58].

This relation can be modified yet further. Assume that the wavelengths of light used are in the optical range, so that only the electronic polarizability of the atoms is active [58]. This means that the dielectric constant ϵ can be replaced by the index of refraction squared $\epsilon = n^2$ [58],

$$\frac{n^2 - 1}{n^2 + 2} = \frac{1}{3\epsilon_0}\sum_j N_j\alpha_j. \tag{3.18}$$

This form is known as the Lorentz-Lorenz equation [46].

For polymeric materials, the Lorentz-Lorenz equation is often written in terms of the density ρ, Avogadro's number N_A, the number of bonds n_j, and the molecular weight of the repeat unit M_0 [46], as

$$\frac{n^2 - 1}{n^2 + 2} = \frac{1}{3\epsilon_0}\sum_j \frac{N_A\rho n_j\alpha_j}{M_0}. \tag{3.19}$$

Robertson and Wilkes used the Lorentz-Lorenz equation as a way to track the changes in density over time of bulk polystyrene from the index of refraction [45]. In order to do this, they had to establish that the physical aging rates calculated from the changes in index of refraction (using refractometry) can be related to the

changes in volume (using volume dilatometry) [45]. Robertson and Wilkes found that the physical aging rate calculated using the Lorentz-Lorenz equation (based on index of refraction measurements) are slightly lower than those calculated using volume dilatometry [45]. It was suspected that there was a possible relationship between the polarizability of the chemical bonds and the density of the film over physical aging, causing this slight decrease in the value of the calculated physical aging rate [45]. However, this method of calculating the physical aging rate using index of refraction measurements and the Lorentz-Lorenz equation was still determined to be a "quantitative alternative" to physical aging rates calculated by monitoring the volume of the polymer [45]. It should be noted that the normalization term $1/L_\infty$ used for Method 3 (Table 3.1) of this thesis originally came from Robertson and Wilkes [45].

Huang and Paul improved upon this method in a few ways. They were the first to use ellipsometry to measure the changes in the index of refraction of polymer films due to physical aging [23]. They used the Lorentz-Lorenz equation (Eq. (3.1)) as a way to calculate the physical aging rate of their polymer films. Since use of the Lorentz-Lorenz equation to calculate physical aging rates was already established by Robertson and Wilkes [45], this is a perfectly reasonable method to analyze the physical aging of their polymer films. Based on the physical aging rates calculated from the Lorentz-Lorenz equation, physical aging was found to proceed faster in thinner polymer films compared to thicker ones in agreement with their gas permeation measurements [23].

3.2.4 Method 4 Index of Refraction

The fourth aging method uses the change in the index of refraction with logarithmic time as well as the change in film thickness and index of refraction with temperature

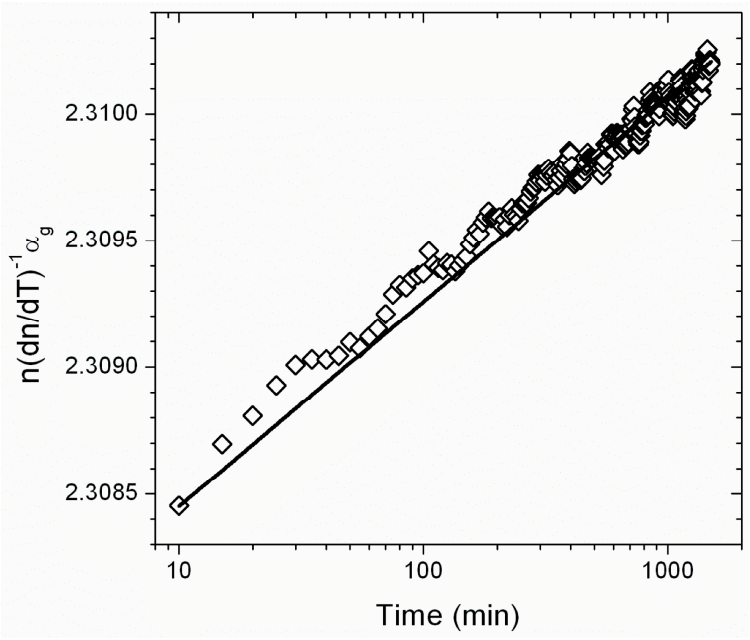

Figure 3.9: This graph shows the change in the product of the index of refraction, the inverse of the dependence of the index of refraction on temperature in the glassy state, and the calculated thermal expansion coefficient of the glassy state of PS plotted against logarithmic time for a representative 2.58 μm PS film supported on silicon aged for 24 hours at 75 °C The slope of the line fit to this data produces the physical aging rate β (Method 4, Table 3.1).

in the glassy state to determine the physical aging rate (Method 4, Table 3.1) [45],

$$\beta_4 = \left(\frac{\partial n}{\partial \log t}\right)_{P,T} \left(\frac{\partial n}{\partial T}\right)^{-1}_{P,t} \alpha_g, \tag{3.20}$$

where the thermal expansion coefficient of the glassy polymer can be written as [45],

$$\alpha_g = -\frac{1}{h_\infty}\left(\frac{\partial h}{\partial T}\right)_{glassy,P,T}. \tag{3.21}$$

The index of refraction multiplied by dn/dT and α_g is plotted against logarithmic time in Figure 3.9. The data taken for this graph was from a 2.58 μm PS film supported on native silicon aged at 75 °C for 24 hours. The slope from this graph produces the physical aging rate for Method 4 (Table 3.1).

Robertson and Wilkes were able to derive this method from Struik's original definition of physical aging [6, 45]. Beginning with Struik's formula, [6, 45],

$$\beta = -\frac{1}{V_\infty}\left(\frac{\partial V}{\partial \log t}\right)_{P,T}, \tag{3.22}$$

and using the chain rule, this expression can be split into separate components,

$$\beta = -\left(\frac{\partial n}{\partial \log t}\right)_{P,T} \left(\frac{\partial T}{\partial n}\right)_{P,t} \frac{1}{V_\infty}\left(\frac{\partial V}{\partial T}\right)_{P,t}. \tag{3.23}$$

The last two terms on the right hand side are the expression of the thermal expansion coefficient (the volumetric form of Eq. (3.21)), so the formula finally assumes the form of Method 4, Table 3.1 [45]. The fourth method allows the volumetric physical aging rate to be determined using three components: the change in the index of refraction with logarithmic time, the inverse of the change of the index of refraction with temperature, and the thermal expansion coefficient of the glassy polymer [45]. While Robertson and Wilkes used this method to determine the physical aging rate

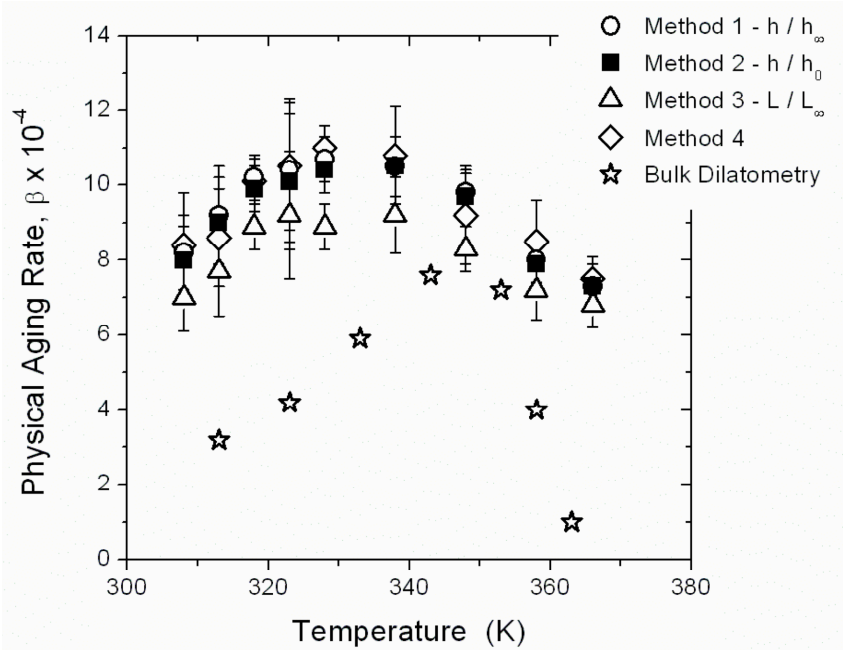

Figure 3.10: This graph depicts the changes in the physical aging rate calculated using Method 1 (circles), Method 2 (squares), Method 3 (upward-pointing triangles), and Method 4 (hollow diamonds) plotted against temperature for PS films ∼2500 nm thick supported on silicon aged for 24 hours. The stars represent dilatometry data for PS measured over 24 hours taken from Greiner and Schwarzl [21]. Qualitatively, each one of the methods produces curves which are similar to the existing bulk volumetric data.

using volume dilatometry studies [45], the form of Method 4 allows determination of each component using ellipsometry. The only component of Method 4 that is actually changing over time is the index of refraction, which an ellipsometer can measure easily. The other constants can also be determined by ellipsometry: the Table in Section 2.3 gives values of dh/dT and dn/dT in the glassy and equilibrium liquid states.

3.3 Comparison of Temperature Dependence of Physical Aging Rate β

All four methods to calculate the physical aging rate have been graphed against temperature in Figure 3.10 (Methods 1-4 from Table 3.1). Each method produces

a physical aging rate characteristic of polystyrene at the given aging temperatures. All four methods produce physical aging rates within error of each other, with the exception of Method 3, which uses the Lorentz-Lorenz equation. This slightly lower physical aging rate was observed and accounted for by Robertson and Wilkes [45]. Of the other three methods, Methods 1, 2, and 4, the first one is expected to be the closest to the original physical aging rate calculation by Struik [6]. Since it is the closest to the original formulation that can be achieved from these ellipsometry measurements, the values of of β are anticipated to be in agreement with bulk dilatometry measurements. Method 4 is a mathematical rearrangement of Method 1, so its physical aging rates will also be expected to be close to bulk dilatometry measurements. In addition, Robertson and Wilkes [45] have experimentally demonstrated agreement between Method 4 and physical aging rates measured by bulk dilatometry. The second method uses a normalization constant h_0 at most a few nanometers different from the calculated theoretical equilibrium film thickness h_∞, so the values of β calculated using this method should be similar to those from Methods 1 and 4. Considering that Method 2 produces acceptable results of the physical aging rate more efficiently than the other two methods, it is chosen out of all four methods to be the best method to calculate the physical aging rate of a polymer film for this thesis.

Comparison of the calculated physical aging rates (Methods 1-4, Table 3.1) to bulk dilatometry measurements by Greiner and Schwarzl in Figure 3.10 show that the curves calculated using the new ellipsometry method of Section 2.4 produce physical aging rate vs. temperature curves similar in shape to those of bulk dilatometry measurements [21]. However, the physical aging rates calculated via the four methods produce physical aging curves consistently higher than those of Greiner and Schwarzl [21]. It is important to remember that the films in this experiment are quenched in a supported state, and can contract in only one dimension. Dilatometry measurements are performed on bulk samples (on the order of mm [21]), and can contract in three

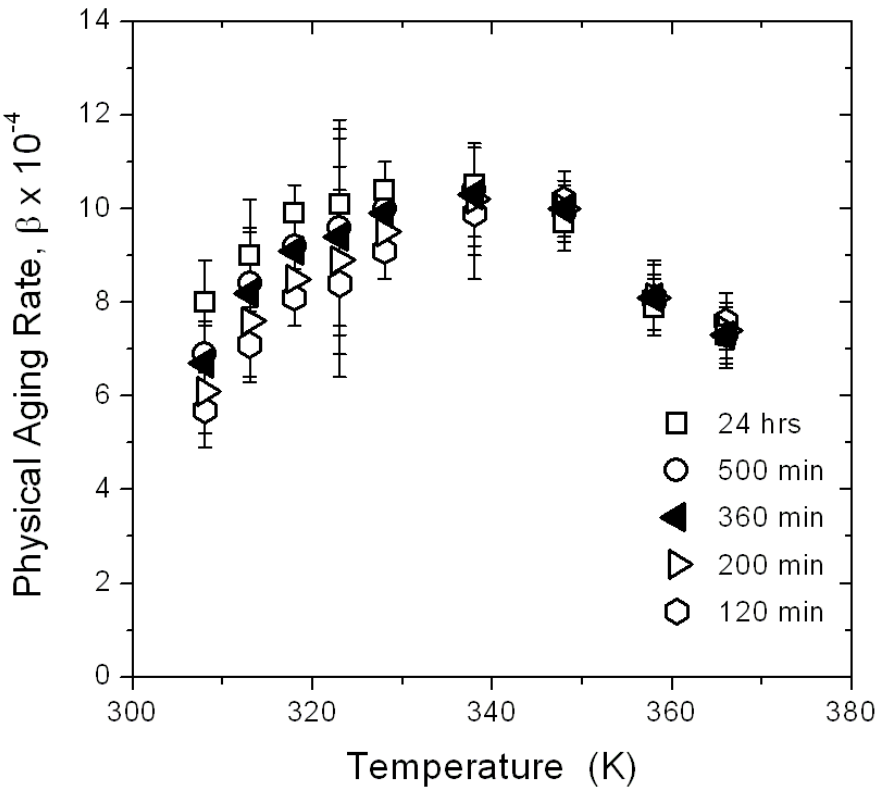

Figure 3.11: This graph shows the changes in the physical aging rate plotted against temperature for ∼2500 nm PS films supported on silicon analyzed via Method 2 (Table 3.1) for five different aging times: 24 hours (squares) [7, 21], 500 minutes (circles) [29, 30, 33, 57], 360 minutes (leftward-pointing triangles) [29, 30, 62], 200 minutes (rightward-pointing triangles) [17], and 120 minutes (hexagons) [30].

dimensions. New measurements performed on PS films quenched in a free-standing state produce physical aging rates that are lower than those in the supported state, and consistent with the values calculated by Greiner and Schwarzl [21,61]. This lends evidence to the idea that the way in which the polymer films are quenched have a direct effect on the way in which they age [61].

3.4 Optimization of Physical Aging Time

The physical aging rate was first calculated over 24 hours (similar to refs. [7, 21]), but has also been reanalyzed for different, shorter amounts of time using Method 2

(Table 3.1). From Hutchinson, it is known that 24 hours of physical aging is long enough to characterize the physical aging rate of PS [7]. A survey of different aging times was taken to discern the optimum time over which to measure physical aging. It was desired that a balance between accurate measurements and experimental time was achieved to optimize experimental efficiency. The existing 24 hour aging rate data were reanalyzed from times starting at t = 0 to 500 minute [29, 30, 33, 57], 360 minute [29, 30, 62], 200 minute [17], and 120 minute [30] lengths of aging time, each consistent with previous aging experiments.

The results of such an analysis are presented in Figure 3.11. As the aging time becomes shorter, the physical aging rate decreases below 65 °C. Above 65 °C, each aging time produces nearly identical physical aging rates. This is because at the lower aging temperatures, more time is needed for the change in film thickness or index of refraction of the polymer plotted against logarithmic time to approach a linear shape instead of a curve. The shortest aging time which produced physical aging rates within one standard deviation of those calculated over 24 hours of aging time was 360 minutes. The new physical aging time was chosen to be 360 minutes.

3.5 Dependence of Physical Aging Rate on Film Thickness

The dependence of physical aging rate on film thickness was tested with supported PS films. This serves two purposes: first, the changes in physical aging rate with film thickness for PS calculated using this new ellipsometry method can be compared to those previously measured by Torkelson and coworkers using fluorescence [30]. Second, it will test the limits of the ellipsometer's ability to measure thinner films. It is known that below ∼30 nm, the ellipsometer is unable to independently resolve film thickness h and index of refraction n [36, 37]. Supported PS films of various

thicknesses from ∼2500 nm to ∼30 nm were aged for 360 minutes at 65 °C, the temperature at which the highest aging rates were recorded in Figure 3.10, using the new experimental ellipsometry technique of this thesis. The change in physical aging rate β (from Method 2, Table 3.1) against film thickness is plotted in Figure 3.12. For film thicknesses ranging from ∼2500 nm to ∼100 nm, there is no change in the physical aging rate with film thickness. However, at film thicknesses smaller than 100 nm, there is a decrease of physical aging rate with decreasing film thickness. The decrease in physical aging rate with film thickness for the thinnest films is in contradiction with physical aging measurements of supported PS films by Torkelson and coworkers [30]. However, they only measured the physical aging of supported PS films at two film thicknesses (500 nm and 20 nm) using fluorescence [30], while the measurements here are more extensive.

There are two different possible explanations for the decrease in physical aging rate with decreasing film thickness for the thinnest films in Figure 3.12. The first possibility is that because the glass transition temperature for PS films less than ∼100 nm is known to decrease with decreasing film thickness [11, 13, 15, 16], it is possible that there would be a corresponding shift in the physical aging rate vs. temperature curve for thinner PS films to the left compared to their bulk counterparts of Figure 3.10. In this case, the peak of the physical aging rate curve would no longer be located at 65 °C, resulting in a decrease in β with decreasing film thickness measured at a constant temperature of 65 °C. A simple shift in $\beta(T)$ corresponding to the shift in T_g to lower values was observed recently in experiments by Koh and Simon on "stacked ultrathin polystyrene films" using differential scanning calorimetry [63]. To test this first possibility, the physical aging rates of (29 ± 1) nm supported PS films were measured as a function of aging temperature, and plotted along with their bulk counterparts in Figure 3.13. From Figure 3.13, it is clear that the physical aging rates of very thin PS films do not simply shift to lower aging temperatures with decreasing

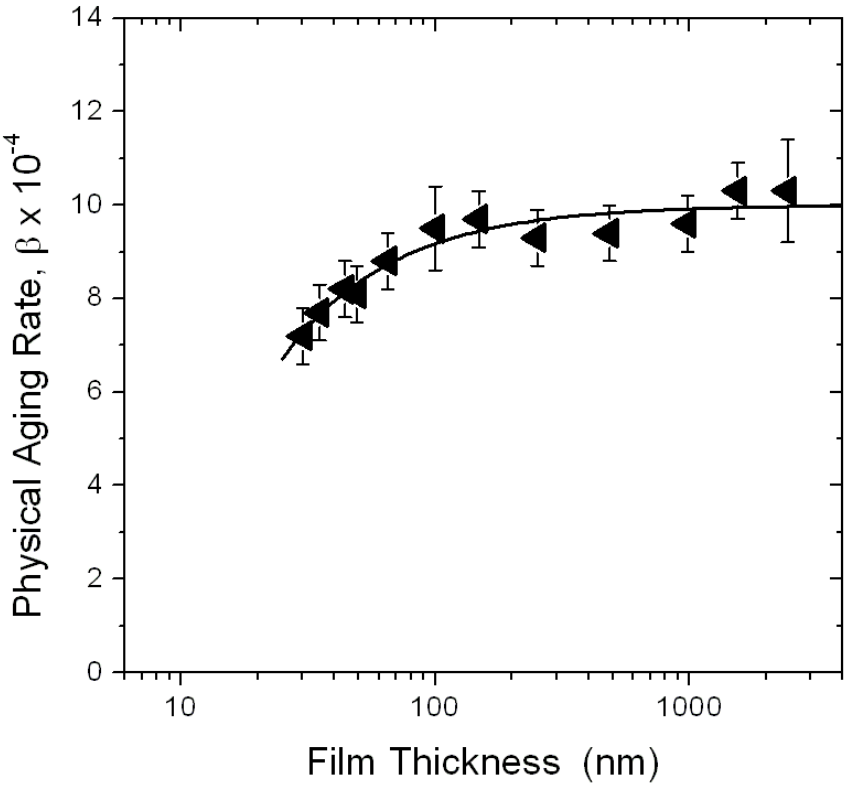

Figure 3.12: This graph shows the physical aging rate β plotted against film thickness measured from supported PS films of film thicknesses ∼30 nm to ∼2500 nm aged at 65 °C for 360 minutes and analyzed via Method 2 (Table 3.1). For film thicknesses ranging from 100 nm to 2500 nm, there is no change in the physical aging rate with film thickness. However, there is a decrease in the physical aging rate with decreasing film thickness for films less than 100 nm thick. The curve fitting the data comes from Equation (3.24).

film thickness. Thus, a simple shift of T_g to lower temperatures does not explain the decrease in the physical aging rate for the thinnest films in Figure 3.12.

The second possible explanation for the decrease in physical aging rate with decreasing film thickness for thinner supported PS films in Figure 3.12 is that there is a gradient in the dynamics of the polymer film. From Ellison and Torkelson's work, it is known that the reduction in T_g is not uniform over the entire film, but rather describes a gradient of T_gs as a function of depth from the free surface with a corresponding gradient in the mobility in each layer of the polymer [16]. Torkelson's group

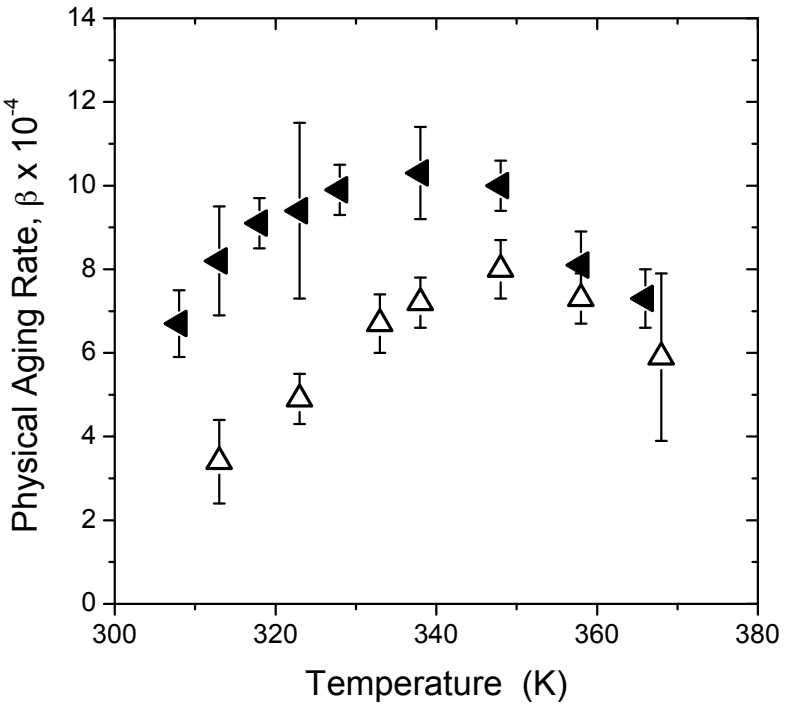

Figure 3.13: This graph shows the data for the physical aging rate β against temperature for bulk supported PS films analyzed over 360 minutes (leftward-pointing triangles), and 30 nm thick PS films (upward-pointing triangles), both analyzed via Method 2 (Table 3.1). The physical aging rates of the 30 nm thick PS films are noticeably decreased compared to their bulk counterparts

went on to demonstrate that there exists a corresponding gradient in the physical aging rate with depth [17]. Therefore, the film could be modeled in layers, each with its own T_g and β, which collectively produce a gradient in dynamics.

Suppose the PS film were modeled not as a single layer but six layers, each with its own T_g and physical aging rate β. The top layer would have the most reduced T_g, while the layer nearest the bottom would have a bulk T_g value, much like in Ellison and Torkelson's work [16]. The resulting physical aging rate measured from such a model using ellipsometry would be a weighted average of each layer [10]. However, only one value of the physical aging rate is measured using ellipsometry. A single measured value cannot solve six unknown parameters. The best that can be done is to model the polymer as a bilayer film, a thin liquidlike layer (no physical aging)

atop a "bulk" layer underneath, similar to what was done by Kawana and Jones [64]. Justin Pye has derived an expression for $\beta(h)$ based on a two layer model [10],

$$\beta(h) = \beta_{bulk}\,(1 - A/h) \tag{3.24}$$

where the best fit to the data of Figure 3.12 results in $\beta_{bulk} = 10 \times 10^{-4}$ and a liquidlike layer A of 8 ± 1 nm thick [10]. A liquidlike layer thickness of 5-10 nm is in agreement with similar estimates by Kawana and Jones [64]. It is not claimed that this bilayer film model is an accurate representation of the dynamics of the polymer film, but it does explain the downturn in the physical aging rate of the polymer film at film thicknesses below 100 nm. The best explanation for the decrease in physical aging rate for the thinnest PS films is that there exists a gradient in the physical aging rate β with depth that at best can be interpreted by the ellipsometer as a bilayer model [10].

Chapter 4

Conclusions and Future Work

4.1 Conclusions

The streamlined ellipsometry procedure developed in this thesis to measure the physical aging rate of confined polymer films is successfully able to characterize the physical aging rate of polystyrene films supported on native silicon. Out of four different methods used to calculate the physical aging rate, the second method (Method 2, $\beta = -(1/h_0)(\partial h/\partial \log t)$) was chosen as the method to be used for future physical aging experiments. The time of the experiment was optimized to 360 minutes, to balance both experimental accuracy and time constraints. Measurements of physical aging rates against film thickness for PS produced no change in the physical aging rate from film thicknesses ranging from $\sim$2.5 μm to 100 nm, but a decrease is observed below 100 nm. Justin Pye has developed a bilayer model to try and explain this decrease in physical aging rate with film thickness [10]. Future work consists of measuring the physical aging of supported films with different polymers and free-standing PS films [61]. The first of these experiments will allow comparison of polymers with flexible C-C backbones and stiff backbones, in accordance with the future scope of this thesis. The second will allow analysis of the effect of the quench (3D vs. 1D) on the physical aging of polymer films.

4.2 Future Work

A number of different directions exist for future work. At the time of completion of this thesis, there were three works in progress for further developing the scope of this thesis. First, experiments measuring the physical aging rate of supported bulk PMMA films (∼2200 nm) vs. aging temperature were begun by Kate Rohald [65]. Preliminary results indicate that the physical aging rates calculated from the new ellipsometry method once again result in curves characteristic of those measured using bulk dilatometry experiments [21]. Second, the physical aging rate of supported PSF films aged at 35 °C of three different film thicknesses (400 nm, 700 nm , 1000 nm) were measured by Kate Rohald to compare with the aging measurements of Huang and Paul [23,65]. This is the first direct test of using the same experimental method (new streamlined ellipsometry procedure) on a polymer with a stiff backbone structure, one of the terms covered in the scope of this thesis. Early results seem to indicate that the supported films offer no change in physical aging rate with film thickness, in contradiction to the results of Huang and Paul [23]. This may have to do with the different methods of thermally quenching between their method and the one presented in this thesis: they quench their films in a free-standing state [2], while the films in the experiments presented in this thesis were quenched in a supported state. Evidence for this concept, that the way in which the films are thermally quenched affects the changes in physical aging with film thickness, was explored by Connie Roth [61]. Connie Roth quenched PS films (two groups, ∼1400 nm and ∼600 nm in thickness) in a free standing state and aged them at 65 °C following the 360 minute streamlined ellipsometry physical aging procedure developed in this thesis [61]. Two significant preliminary results emerged from these experiments: the thicker films (∼1400 nm thick) produced physical aging rates closer to bulk dilatometry values [21], and that the thinner films (∼600 nm thick) aged faster relative to the thicker films [61]. All three of these experiments will serve to further strengthen the importance of the new

streamlined ellipsometry procedure and will allow comparison of polymers based on backbone structure, aging temperature, film thickness, and quench type (3D or 1D).

Chapter 5

Appendix

Written using MATLAB. Elizabeth Baker. 2008.

% This program is designed to calculate the path of light through

% a film on the ellipsometer consisting of a film of film thickness h, a

% silicon oxide layer of height 2 nm, and a silicon layer of height

% 1 mm, sitting in air. With an intake of n, h, and wavelength

% ranges, it will output psi and delta for a rotating compensator

ellipsometer

% Now for the full air, film, SiOx, Si layered substrates.

% This one uses that clever way of manipulating reflection coefficients from

% Azzam and Bashara

fprintf('Wavelength \t Psi \t Delta \t\t ROTATING COMPENSATOR

ELLIPSOMETER \n');

% set up constants

h=500.0; %PS film thickness

A=1.57; % Cauchy parameter "A" for PS

B=0.00745; % Cauchy parameter "B" for PS

C=0.0; % Cauchy parameter "C" for PS

```
phi0=(pi/180.0)*65.0; % angle of incidence degrees to radians
n0=1.00+i*0.0; % Index of refraction of air
h2=2.0; % Height of silicon oxide layer (nm)
% Now to run through the range of wavelengths for the data
Lam_min=400.0;
Lam_max=1000.0;
Lam_step=10.0;
for Lam = Lam_min:Lam_step:Lam_max,
w1=Lam/1000;
n1=A+B/w1^2+C/w1^4-i*0.0; % determine index of refraction of film
n2=1.83591-0.45359*w1+0.78098*w1^2-0.62404*w1^3+0.18914*w1^4;
% Index of refraction of
% silicon oxide layer
n3=(74.24801-471.03945*w1+1263.87875*w1^2-1691.01033*w1^3+1123.2845*w1^4-
295.81095*w^5)+i*(161.26002-1628.03125*w1+6970.26661*w1^2-16398.60047*w1^3+
22895.22659*w1^4-18972.91468*w1^5+8643.0234*w1^6-1670.23284*w1^7); % Index
of refraction of silicon wafer
% Snell's law used to calculate angles of refraction
cos_phi0=cos(phi0);
cos_phi1=sqrt(1-((n0/n1)*sin(phi0))^2);
cos_phi2=sqrt(1-((n0/n2)*sin(phi0))^2);
cos_phi3=sqrt(1-((n0/n3)*sin(phi0))^2);
% Fresnel reflection coefficients;
rp01=(n1*cos_phi0 - n0*cos_phi1)/(n1*cos_phi0 + n0*cos_phi1);
rs01=(n0*cos_phi0 - n1*cos_phi1)/(n0*cos_phi0 + n1*cos_phi1);
rp12=(n2*cos_phi1 - n1*cos_phi2)/(n2*cos_phi1 + n1*cos_phi2);
rs12=(n1*cos_phi1 - n2*cos_phi2)/(n1*cos_phi1 + n2*cos_phi2);
```

```
rp23=(n3*cos_phi2 - n2*cos_phi3)/(n3*cos_phi2 + n2*cos_phi3);
rs23=(n2*cos_phi2 - n3*cos_phi3)/(n2*cos_phi2 + n3*cos_phi3);
% Special constants dealing with transfer from one media to
% another
beta1=2*pi*n1*h*cos_phi1/Lam; %this is the beta for PS
beta2=2*pi*n2*h2*cos_phi2/Lam; %beta for SiOx
% Formula for total relfection coefficients
rptot23=(rp12+rp23*exp(-2*i*beta2))/(1+rp12*rp23*exp(-2*i*beta2));
rstot23=(rs12+rs23*exp(-2*i*beta2))/(1+rs12*rs23*exp(-2*i*beta2));
rptot12=(rp01+rptot23*exp(-2*i*beta1))/(1+rp01*rptot23*exp(-2*i*beta1));
rstot12=(rs01+rstot23*exp(-2*i*beta1))/(1+rs01*rstot23*exp(-2*i*beta1));
% get rho
rho = rptot12/rstot12;
% now get Psi and Delta
Psi = atan(abs(rho))*180.0/pi;
%Delta = atan(imag(rho)/real(rho))*180.0/pi;
Delta = angle(rho)*180.0/pi;
if Delta <= -90,
Delta = Delta + 360; % The 360 is just a phase shift.
end
%print out results
fprintf('%g \t %g \t %g \n',Lam,Psi,Delta);
% store values of psi and delta for plotting
k=(Lam-Lam_min)/Lam_step+1;
Wavelengths(k)=Lam;
PsiArray(k)=Psi;
DeltaArray(k)=Delta;
```

```
end
% now plot
plot(Wavelengths,PsiArray,Wavelengths,DeltaArray);
xlabel('Wavelength(nm)');
ylabel('Psi (blue) and Delta (green)');
```

Bibliography

[1] R. D. Priestley, "Physical aging of confined glasses," *Soft Matter*, vol. 5, pp. 919–926, 2009.

[2] Y. Huang and D. R. Paul, "Experimental methods for tracking physical aging of thin glassy polymer films by gas permeation," *Journal of Membrane Science*, vol. 244, pp. 167–178, 2004.

[3] H. Richardson, I. Lopez-Garcia, M. Sferrazza, and J. L. Keddie, "Thickness dependence of structural relaxation in spin-cast, glassy polymer thin films," *Phys. Rev. E.*, vol. 70, p. 051805, 2004.

[4] P. C. Hiemenz and T. P. Lodge, *Polymer Chemistry: Second Edition*. Taylor & Francis Group, LLC, 2007.

[5] C. A. Angell, K. L. Ngai, G. B. McKenna, P. F. McMillan, and S. W. Martin, "Relaxation in glassforming liquids and amorphous solids," *J. Appl. Phys.*, vol. 88, pp. 3113–3157, 2000.

[6] L. C. E. Struik, *Physical Aging in Amorphous Polymers and Other Materials*. Elsevier Scientific Publishing Company, 1978.

[7] J. M. Hutchinson, "Physical aging of polymers," *Prog. Polym. Sci.*, vol. 20, pp. 703–760, 1995.

[8] S. Simon, *Encyclopedia of Amorphous Polymers and Other Materials*. John Wiley & Sons, 2002.

[9] I. M. Hodge, "Physical aging in polymer glasses," *Science*, vol. 267, pp. 1945–1947, 1995.

[10] E. A. Baker, P. Rittigstein, K. A. Rohald, J. E. Pye, J. M. Torkelson, and C. B. Roth, "Streamlined ellipsometry procedure for characterizing physical aging rates of thin polymer films," *Journal of Polymer Science Part B: Polymer Physics*, Submitted 01 Jun 2009.

[11] J. L. Keddie, R. A. L. Jones, and R. A. Cory, "Size-dependent depression of the glass transition temperature in polymer films," *Europhysics Letters*, vol. 27, pp. 59–64, 1994.

[12] J. L. Keddie, R. A. L. Jones, and R. A. Cory, "Interface and surface effects on the glass-transition temperature in thin polymer films," *Faraday Discussions*, vol. 98, pp. 219–230, 1994.

[13] K. Dalnoki-Veress, J. A. Forrest, C. Curray, C. Gigault, and J. R. Dutcher, "Molecular weight dependence of reductions in the glass transition temperature of thin, freely-standing polymer films," *Phys. Rev. E.*, vol. 63, p. 031801, 2001.

[14] C. B. Roth, K. L. McNerny, W. F. Jaeger, and J. M. Torkelson, "Eliminating the enhanced mobility at the free surface of polystyrene: Fluorescence studies of the glass transition temperature in thin bilayer films of immiscible polymers," *Macromolecules*, vol. 40, pp. 2569–2574, 2007.

[15] C. B. Roth and J. R. Dutcher, "Glass transition and chain mobility in thin polymer films," *Journal of Electroanalytical Chemistry*, vol. 584, pp. 13–22, 2005.

[16] C. J. Ellison and J. M. Torkelson, "The distribution of glass-transition temperatures in nanoscopically confined glass formers," *Nature Materials*, vol. 2, pp. 695–700, 2003.

[17] R. D. Priestley, C. J. Ellison, L. J. Broadbelt, and J. M. Torkelson, "Structural relaxation of polymer glasses at surfaces, interfaces, and in between.," *Science.*, vol. 309, pp. 456–459, 2005.

[18] Y. Huang, X. Wang, and D. R. Paul, "Physical aging of thin glassy polymer films: Free volume interpretation," *Journal of Membrane Science*, vol. 277, pp. 219–229, 2006.

[19] Y. Huang and D. R. Paul, "Effect of film thickness on the gas-permeation characteristics of glassy polymer membranes," *Ind. Eng. Chem. Res.*, vol. 46, pp. 2342–2347, 2007.

[20] S. L. Simon, J. W. Sobieski, and D. J. Plazek, "Volume and enthalpy recovery of polystyrene.," *Polymer*, vol. 42, pp. 2555–2567, 2001.

[21] R. Greiner and F. R. Schwarzl, "Thermal contraction and volume relaxation of amorphous polymers," *Rheologica Acta*, vol. 23, pp. 378–395, 1984.

[22] Y. Huang and D. R. Paul, "Effect of molecularweight and temperature on physical aging of thin glassy poly(2,6-dimethyl-1,4-phenylene oxide) films," *Journal of Polymer Science: Part B: Polymer Physics*, vol. 45, pp. 1390–1398, 2007.

[23] Y. Huang and D. R. Paul, "Physical aging of thin glassy polymer films monitored by optical properties," *Macromolecules*, vol. 39, pp. 1554–1559, 2006.

[24] Y. Huang and D. R. Paul, "Effect of temperature on physical aging of thin glassy polymer films," *Macromolecules*, vol. 38, pp. 10148–10154, 2005.

[25] Y. Huang and D. R. Paul, "Physical aging of thin glassy polymer films monitored by gas permeability," *Polymer*, vol. 45, pp. 8377–8393, 2004.

[26] P. H. Pfromm and W. J. Koros, "Accelerated physcial aging of thin glassy polymer-films–evidence from gas-transport measurements," *Polymer*, vol. 36, pp. 2379–2387, 1995.

[27] K. D. Dorkenoo and P. H. Pfromm, "Experimental evidence and theoretical analysis of physical aging in thin and thick amorphous glassy polymer films," *Journal of Polymer Science: Part B: Polymer Physics*, vol. 37, pp. 2239–2251, 1999.

[28] M. S. McCaig and D. R. Paul, "Effect of film thickness on the changes in gas permeability of a glassy polyarylate due to physical aging part 1. experimental observations," *Polymer*, vol. 41, pp. 629–637, 2000.

[29] C. J. Ellison, S. D. Kim, D. B. Hall, and J. M. Torkelson, "Confinement and processing effects on glass transition temperature and physical aging in ultrathin polymer films: Novel fluorescence measurements," *European Physical Journal E*, vol. 8, pp. 155–166, 2002.

[30] R. D. Priestley, L. J. Broadbelt, and J. M. Torkelson, "Physical aging of ultrathin polymer films above and below the bulk glass transition temperature: Effects of attractive vs. neutral polymer-substrate interactions measured by fluorescence," *Macromolecules*, vol. 38, pp. 654–657, 2005.

[31] R. D. Priestley, P. Rittigstein, L. J. Broadbelt, K. Fukao, and J. M. Torkelson, "Evidence for the molecular-scale origin of the suppression of physical ageing in confined polymer: Fluorescence and dielectric spectroscopy studies of polymer-silica nanocomposites," *Journal of Physics–Condensed Matter*, vol. 19, p. 205120, 2007.

[32] Y. Yampolskii, I. Pinnau, and B. Freeman, eds., *Materials Science of Membranes for Gas and Vapor Separation*. John Wiley & Sons, 2006.

[33] P. Rittigstein and J. M. Torkelson, "Polymernanoparticle interfacial interactions in polymer nanocomposites: Confinement effects on glass transition temperature and suppression of physical aging," *Journal of Polymer Science: Part B: Polymer Physics*, vol. 44, pp. 2935–2943, 2006.

[34] J. S. Royal and J. M. Torkelson, "Physical aging effects on molecular-scale polymer relaxations monitored with mobility-sensitive fluorescent molecules," *Macromolecules*, vol. 26, pp. 5331–5335, 1993.

[35] E. Hecht, *Optics, 4th Edition*. Pearson Education, Inc., 2002.

[36] H. G. Tompkins and E. A. Irene, *Handbook of Ellipsometry*. William Andrew Publishing/Noyes, 2005.

[37] H. G. Tompkins, *A User's Guide to Ellipsometry*. Dover Publications, Inc., 1993.

[38] J. A. Woollam, Inc., *Guide to Using WVase32*, 2007.

[39] E. Collett, *Polarized Light: Fundamentals and Applications*. Marcel Dekker, Inc., 1993.

[40] J. Brandup, E. H. Immergut, E. A. Grulke, R. J. Andrews, A. Abbe, and D. R. Bloch, *Polymer Handbook: 4th Edition*. John Wiley & Sons, Inc., 1999.

[41] C. M. Herzinger, B. Johs, W. A. McGahan, and J. A. Woollam, "Ellipsometric determination of optical constants for silicon and thermally grown silicon dioxide via a multi-sample, multi-wavelength, multi-angle investigation," *J. Appl. Phys.*, vol. 83, pp. 3323–3336, 1998.

[42] R. M. A. Azzam and N. M. Bashara, *Ellipsometry and Polarized Light*. Elsevier Science Publishers B. V., 1987.

[43] M. D. Millan, J. Locklin, T. Fulghum, A. Baba, and R. C. Advincula, "Polymer thin film photodegradation and photochemical crosslinking: FTIR imaging, evanescent waveguide spectroscopy, and QCM investigations," *Polymer*, vol. 46, pp. 5556–5568, 2005.

[44] C. A. Angell, "Formation of glasses from liquids and biopolymers," *Science*, vol. 267, pp. 1924–1935, 1995.

[45] C. G. Robertson and G. L. Wilkes, "Refractive index: A probe for monitoring volume relaxation during physical aging of glassy polymers," *Polymer*, vol. 39, pp. 2129–2133, 1998.

[46] N. J. Mills, *Encyclopedia of Polymer Science and Engineering*, vol. 10. John Wiley & Sons, Inc., 2nd ed., 1987.

[47] G. B. McKenna, "Glassy states: Concentration glasses and temperature glasses compared," *Journal of Non-Crystalline Solids*, vol. 353, pp. 3820–3828, 2007.

[48] Y. Zheng and G. B. McKenna, "Structural recovery in a model epoxy: Comparison of responses after temperature and relative humidity jumps," *Macromolecules*, vol. 36, pp. 2387–2396, 2003.

[49] A. J. Kovacs, "Glass transition in amorphous polymers," *Forschr. Hochpolym.-Forch*, vol. 3, pp. 394–507, 1963.

[50] P. A. Rodgers, "Pressure-volume-temperature relationships for polymeric liquids: A review of equations of state and their characteristic parameters for 56 polymers," *Journal of Applied Polymer Science*, vol. 48, pp. 1061–1080, 1993.

[51] J. H. Dymond and R. Malhorta, "The tait equation: 100 years on," *International Journal of Thermophysics*, vol. 9, pp. 941–951, 1988.

[52] A. Quach and R. Simha, "Pressure volume temperature properties and transition of amorphous polymers polystyrene and poly(orthomethylstyrene)," *Journal of Applied Physics*, vol. 42, pp. 4592–4606, 1971.

[53] A. Hiltner, R. Y. F. Liu, Y. S. Hu, and E. Baer, "Oxygen transport as a solid-state structure probe for polymeric materials: A review," *Journal of Polymer Science: Part B: Polymer Physics*, vol. 43, pp. 1047–1063, 2005.

[54] R. G. Larson, *The Structure and Rheology of Complex Fluids*. Oxford University Press, 1999.

[55] J. S. Vrentas and J. L. Duda, "A free-volume interpretation of the influence of the glass transition on diffusion in amorphous polymers," *Journal of Applied Polymer Science*, vol. 22, pp. 2325 – 2339, 1978.

[56] A. A. Miller, "Analysis of melt viscosity and glass transition of polystyrene," *Journal of Polymer Science Part A2–Polymer Physics*, vol. 6, pp. 1161–1175, 1968.

[57] P. Rittigstein, R. D. Priestley, L. J. Broadbelt, and J. M. Torkelson, "Model polymer nanocomposites provide an understanding of confinement effects in real nanocomposites," *Nature Materials*, vol. 6, pp. 278–282, 2007.

[58] C. Kittel, *Introduction to Solid State Physics. 7th Edition*. John Wiley & Sons, 1996.

[59] A. R. Blythe and D. Bloor, *Electrical Properties of Polymers*. Cambridge University Press, 2005.

[60] M. A. Omar, *Elementary Solid State Physics: Revised Printing*. Addison Wesley Publishing Company, 1993.

[61] C. B. Roth, "Significance of free-standing vs. supported quench in subsequent physical aging of thin polymer films," *Polymer Preprints*, vol. 50, pp. 792–793, 2009.

[62] J. S. Royal and J. M. Torkelson, "Monitoring the molecular scale effects of physical aging in polymer glasses with fluorescence probes.," *Macromolecules*, vol. 23, pp. 3536–3538, 1990.

[63] Y. P. Koh and S. L. Simon, "Structural relaxation of stacked ultrathin polystyrene films," *Journal of Polymer Science Part B–Polymer Physics*, vol. 46, pp. 2741–2753, 2008.

[64] S. Kawana and R. A. L. Jones, "Effect of physical ageing in thin glassy polymer films," *European Physical Journal B*, vol. 10, pp. 223–230, 2003.

[65] K. Rohald, "Final report," tech. rep., Emory University, Spring 2009.